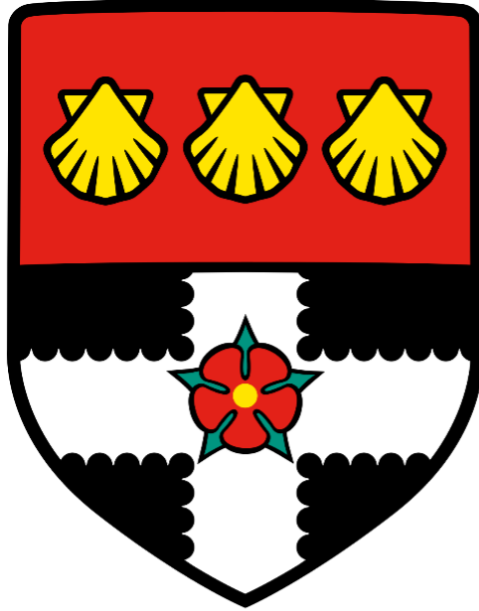


UNIVERSITY OF READING

Department of Meteorology



ORGANISED CONVECTION AND
MESOSCALE CONVECTIVE SYSTEMS IN
THE MARITIME CONTINENT

MC Benoist

A dissertation submitted in partial fulfilment of the requirement for the
degree of Master of Science in Atmosphere, Ocean and Climate

August 2024

Acknowledgements

This dissertation would not have been possible without the continual support and advice of my supervisors, Dan Shipley, Mark Muetzelfeldt and Bob Plant.

Abstract

Convection, particularly from mesoscale convective systems, is responsible for the majority of the precipitation seen in the Maritime Continent, yet convection-permitting models often do a poor job accurately predicting the locations, timings and characteristics of convective activity within the region. In this study, two convection-permitting models are compared with each other and against observations to assess their strengths and weaknesses in modelling mesoscale convective system characteristics and behaviour under three main modes of variability affecting the tropics.

Contents

1	Introduction	1
1.a	Overview of Convection	2
1.b	Organisation of Convection and Mesoscale Convective Systems	5
1.c	The Main Modes of Variability in the Maritime Continent	8
1.d	MJO	9
1.e	ENSO	10
2	Data	11
3	Sensitivity to Definitions	13
4	General Characteristics of MCSs in the Maritime Continent	15
4.a	Spatial Distribution	15
4.b	Fraction of Precipitation Associated with MCSs	17
4.c	Area and Maximum Precipitation	18
5	Diurnal Cycle	19
5.a	Diurnal Cycle Methods	19
5.b	Diurnal Cycle Results and Analysis	20
6	The Madden-Julian Oscillation (MJO)	31
6.a	MJO Methods	31
6.b	MJO Results and Analysis	32
7	El Niño Southern Oscillation (ENSO)	40
7.a	ENSO Methods	40
7.b	ENSO Results and Analysis	41
8	Further Work	47
9	Conclusions	47
	References	50
10	Appendix A: Applicability of Hypothesis Test	54
11	Appendix B: Statistical MCS Forecasting Model Concept	56

1. Introduction

Convection in the atmosphere occurs over a wide range of spatial and temporal scales. Some forms of convection are relatively small, for example single cell cumulonimbus clouds (of length scale 10km), and are frequently responsible for showers globally. Despite not posing much risk to people in comparison to larger systems, they are still of great importance in heat, momentum and moisture budgets. In the tropics, cells often organise, becoming mesoscale convective systems (MCSs), of length scales 100km-1000km. These are responsible for much of the total precipitation seen in the tropics, while bringing additional hazards such as frequent lightning, strong winds, and hail. Despite the importance of convection, models often do a poor job of accurately portraying it. The Maritime Continent in particular is of interest when studying convection modelling, due to the large variety in orographic features, combined with shallow, warm oceans. This study compares two convection models, one using an explicit scheme, and one using a parameterised scheme, with each other and available observations to determine the strengths and weaknesses of each in the modelling of MCSs in the Maritime Continent.

The Maritime Continent is located between 20° north and south, 85° west and 160° east. Given its proximity to the equator, the oceans surrounding the islands are warm, with the surface temperature of the islands increasing fast during the day. Since surface temperature is a large driver of deep convection, this leads to organised systems such as mesoscale convective systems being common in the region. Figure 1 shows the bathymetry of the Maritime Continent.

It shows that, to the south-west and north-east of the domain, there are large areas of deep water. It can be expected that the temperature in this region varies on a slow basis, due to the high heat capacity of water. In contrast, in the centre of the domain and near the islands, the ocean is extremely shallow. The sea south of Borneo, the Java Sea, in particular has an average depth of 46m. This shallow water could be influenced more strongly by factors such as external heating.

Many areas on land are relatively low-lying, however there are some mountain ranges and other orographic features that could influence convective activity. For example, the tallest peak in Papua New Guinea is over 4,500m, with several peaks in the ridge over 3,000m. The forced lifting of air approaching the mountains could lead to the LFC being approached, and lead to the initiation of a convective system.

Given that Sumatra, Java and Papua New Guinea are surrounded on at least one side by open ocean, the prevailing winds of these islands are relatively consistent. On the other hand, Borneo is more complex. It is surrounded on all sides by warm, shallow ocean and other islands with varied topographic features, which could lead to more variable

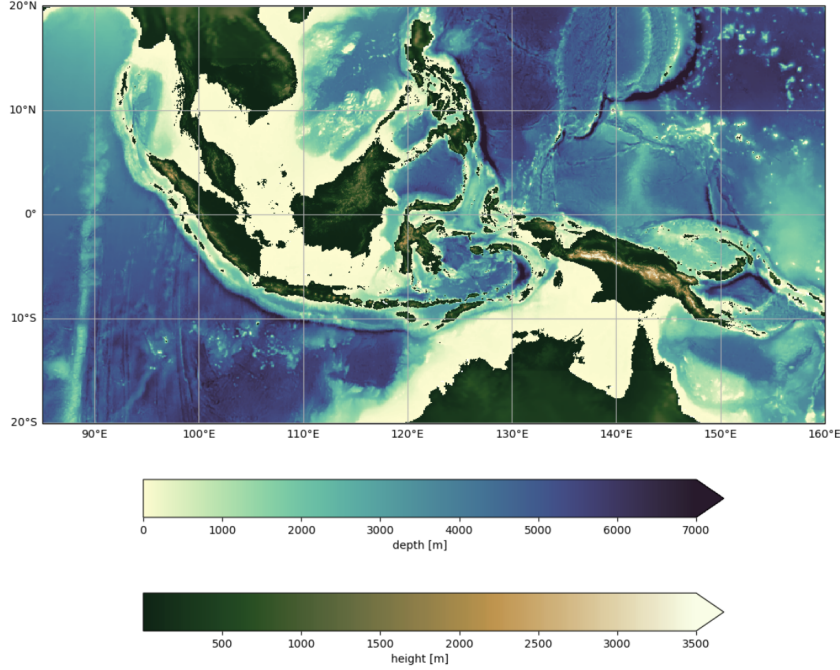


Figure 1: Bathymetry plot of the Maritime Continent. Note the scale for the ocean is twice that of the land

conditions and difficulties in modelling.

Considering again the location of the Maritime Continent in the Tropics and the length of the period over which this study is conducted, 10 years Boreal Winter, it can be hypothesised that organised convection, and more specifically MCSs, will vary less on an intraseasonal basis, but instead may be heavily affected by other modes of variability: the diurnal cycle, the Madden-Julian Oscillation (MJO), and the El-Niño Southern Oscillation (ENSO).

1.a *Overview of Convection*

Vertical instability over a given atmospheric layer occurs when potential temperature θ decreases with height, $\frac{\partial\theta}{\partial z} < 0$, where potential temperature is defined as the temperature a parcel would have if brought adiabatically to some reference pressure, usually taken as surface pressure. Convection can then be thought of as vertical motion arising in these conditions to remove this instability, by bringing surface parcels with high θ upwards.

The lifting condensation level (LCL) is defined as the height at which a parcel lifted adiabatically becomes saturated; the level of free convection (LFC) is the height at which a parcel lifted moist pseudoadiabatically from the LCL to the point where it is warmer than the environment (at this point it is able to ascend); the level of neutral buoyancy (LNB) is the height at which the rising parcel has the same temperature as the environment, and

no longer is positively buoyant. It is still possible for a parcel to rise beyond this point if it has sufficient momentum, resulting in convective overshoot.

Convective available potential energy (CAPE) and convective inhibition (CIN) are quantified by the temperature difference between the parcel and environment, integrated between the LNB and LFC, and the LFC and LCL respectively:

$$CAPE = \int_{LFC}^{LNB} B dz \quad (1)$$

$$CIN = - \int_0^{LFC} B dz \quad (2)$$

where B is buoyancy of a parcel [Markowski and Richardson \(2010\)](#). For deep convection to occur, parcels need to attain positive buoyancy over a large vertical extent after reaching the LFC, indicating that large CAPE is a necessary, but insufficient, condition. CIN acts to prevent the ascent of parcels at the surface, so for deep convection to occur, any CIN present needs to be overcome. This occurs through forced ascent, for example as air is pushed upwards over a cold front, or orographic features such as mountains. In both cases, air at the surface can be forced to rise up to the LFC, resulting in its continued ascent, and potentially deep convection.

The removal of CIN by itself is insufficient for deep convection; soundings showing an abundance of CAPE and no CIN, yet where convection was observed to be absent, could indicate conditions where sounding was taken were not representative of wider environmental conditions.

Calculations can suffer similar problems, with convection generally being overestimated. This is due to the assumption that θ and water vapour mixing ratio r_v are conserved (for the layer between the surface and LCL), when in reality entrainment dilutes the parcel with dry air, resulting in an LCL and LFC that is higher than would be the case in the absence of entrainment. Recently, [Peters et al. \(2023\)](#) derived an expression for a quantity similar to CAPE, but that additionally accounts for entrainment, ECAPE. They found that ECAPE was better able to anticipate the strength of a thunderstorm updraft, and showed promise for use in the prediction of thunderstorm-related hazards, such as hail.

Locations favouring convection can be shown to correlate with locations of moisture convergence, as moisture convergence implies (horizontal) mass convergence, thus upward vertical motion and a deepening of a moist boundary layer.

While theory suggests convection occurs along boundaries where forced ascent is occurring (for example along cold fronts), observations show that convection is confined to sections of the boundary, with gaps in between. Possible explanations include thermo-

dynamic or kinematic inhomogeneities, for example mesocyclones resulting in regions of locally low convergence [Markowski and Richardson \(2010\)](#).

Atmospheric modelling of convection can either be done explicitly or with a parameterisation scheme.

Explicit methods need a small spatial grid length to be able to resolve convection cells. Successfully doing so can give a realistic representation of the location and severity of convection, however it is computationally expensive to resolve convection explicitly, so, particularly when considering large spatial or time scales, convective parameterisation is often used.

Convective parameterisation is a method used to consider larger scales (eg a domain of orders of 1000s of km). It is frequently used in climate models, as running these over a long time period at a fine enough resolution for explicit convection would be extremely expensive. Although downgradient closure is frequently used in general parameterisation schemes, convection does not transport downgradient, so a different approach must be considered.

Velocity, thermodynamic and moisture variables (eg $\langle \mathbf{u} \rangle$) are averaged across the grid box. The grid box itself is composed of regions of deep convective clouds and much larger regions of no convection, and the variables can be broken down in the same way: $\langle \mathbf{u} \rangle = \sigma_c \langle \mathbf{u} \rangle_c + \sigma_e \langle \mathbf{u} \rangle_e$, where σ_c and σ_e are the proportions of convective and environmental area respectively, and $\sigma_c \ll \sigma_e$; $\sigma_c + \sigma_e = 1$.

The accuracy of models is sensitive to the way entrainment, E , is parameterised. Vertical mass flux is considered in form

$$\frac{\partial M}{\partial z} = E - D \quad (3)$$

where D is detrainment. Frequently, the assumption is made that M takes the form $M = M_0(t)m(z)$ so that the time and spatial scales can be separated. Defining fractional entrainment and detrainment as $\epsilon = \frac{E}{M}$ and $\delta = \frac{D}{M}$ respectively such that

$$\frac{\partial m}{\partial z} = \epsilon - \delta \quad (4)$$

The model used to generate results in this report considers a coupled atmosphere and mixed layer ocean, and compares explicit convection (2km grid spacing) and parameterised convection (12km grid spacing).

For both explicit and parameterised convection, vertical profiles of heating and moistening can be considered. In both cases, five groups where profiles are similar emerged: shallow, congestus, deep, and two types of anvil, separated by the extent of re-evaporation.

Comparison of the MC2 and MC12 heating profiles show that while there are some

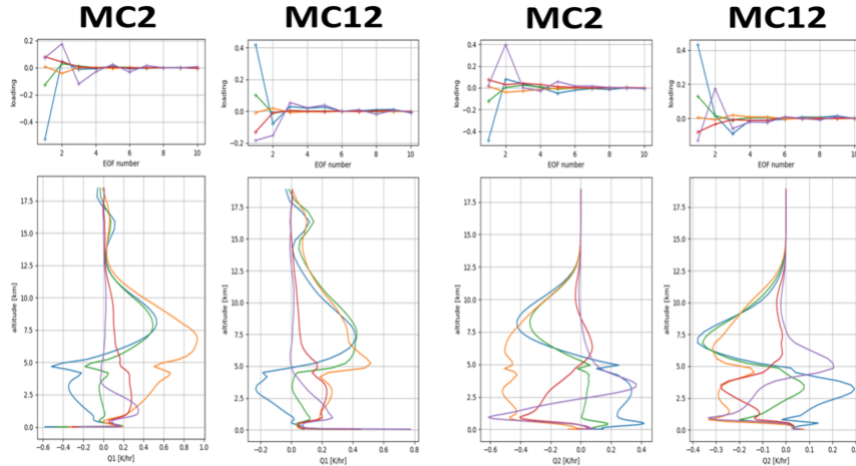


Figure 2: Vertical profiles of heating and moistening variables for clusters (yellow: deep, green: anvil, blue: anvil with re-evaporation, red: congestus, purple: shallow)

similarities in their shapes, such as a region of increased heating above a melting layer for the anvil and deep convection clusters, MC12 often underestimates the magnitude of the heating.

Similarly, the magnitude of moistening is frequently underestimated in MC12. In addition, the shapes of the profiles are more inconsistent. Most notably, MC12 shows a sudden moistening in the layer just below 5km, whereas MC2 shows a slight drying in the same layer.

1.b *Organisation of Convection and Mesoscale Convective Systems*

The magnitude of the 0-6km vertical wind shear, defined as the difference between wind vectors at two given levels, is important in determining storm type, with the low-level shear being particularly important. An environment with moderate shear (10-20m/s) encourages organisation of longer-lived, more severe storms firstly by reducing the weakening of updrafts by precipitation and outflow. Secondly, the gust front is more able to lift air to the LFC, allowing for repeated triggering of new cells as old ones decay, resulting in a more long-lived system.

If the difference, ΔU , between the mean 0-6km wind and the mean 0-500m wind represents storm-relative wind, then the quantity $\frac{1}{2}(\Delta U)^2$ represents the kinetic energy of the inflow [Markowski and Richardson \(2010\)](#). Since CAPE itself can be thought of as a way to quantify the strength of a system's outflow, the ratio between CAPE and inflow kinetic energy, defined as the bulk Richardson number, BRN:

$$BRN = \frac{CAPE}{\frac{1}{2}(\Delta U)^2} \quad (5)$$

gives an indication of how the strength of the inflow and outflow compare [Markowski and Richardson \(2010\)](#). More severe, longer-lived storms occur when these are of similar magnitude, i.e small BRN (≤ 50). For systems with a BRN much larger than 50, the outflow will overwhelm the inflow, and the system will be short-lived [Markowski and Richardson \(2010\)](#).

Mesoscale convective systems (MCSs) are defined by the presence of precipitation of length scale at least 100km in at least one horizontal direction [Houze Jr. \(2004\)](#). They can be further classified by their appearance on radar; for example squall lines have a linear appearance, with the majority being composed of leading convective precipitation, with a wide area of stratiform precipitation, which frequently trails the region of convective precipitation [Houze Jr. \(2004\)](#).

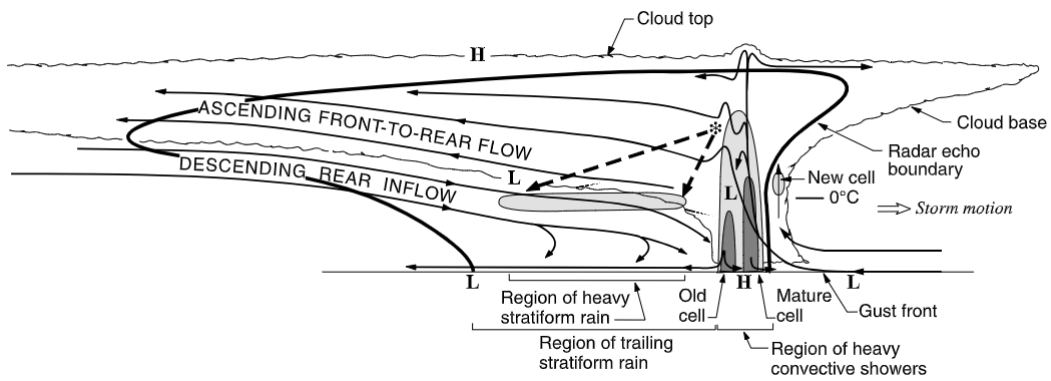


Figure 3: Structure of an MCS, showing regions of convective and stratiform precipitation, and regions of ascending and descending air, reproduced from [Houze Jr. \(2004\)](#)

[Muetzelfeldt et al. \(2024\)](#) discussed how environmental conditions evolve over the course of an MCS’s development and lifetime, as well as the predictability of MCS development from a given environmental condition.

Generally, CAPE increases to a maximum at initiation, and decreases afterwards. CAPE also takes higher values over equatorial and tropical regions, and over the sea when compared to land around the same latitude. Meanwhile, as outlined in the previous section, CIN decreases up to initiation. Notably, CIN is not generally as large over oceans, indicating that it may be easier for large, convective systems to form here in the presence of large CAPE. However, convective systems over land may be aided in their formation by lifting from orographic features such as mountains, and strong surface heating during the day.

5 shows three environmental variables identified by [Muetzelfeldt et al. \(2024\)](#) as being important for MCS formation. Total column water vapour (TCWV) reaches a peak in MCS probability towards higher values, however for oceanic cases, the probability of MCS occurrence significantly decreases past this peak, while MCS probability over land remains

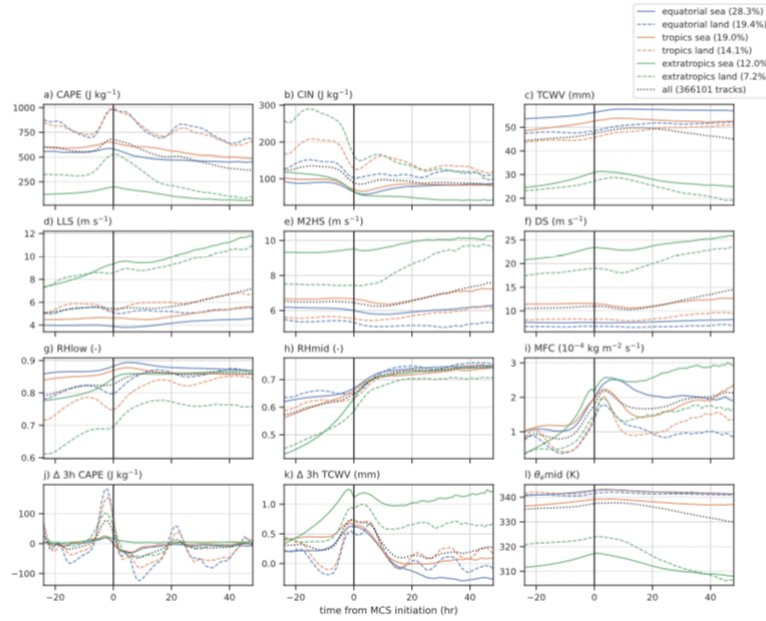


Figure 4: Evolution of environmental variables over MCS lifetime, time 0 being initiation. Reproduced from [Muetzelfeldt et al. \(2024\)](#)

roughly level, at around 0.7. There may be some physical reason why this is, however it was noted that since such high values of TCWV are exceedingly rare, and so this profile could be a result of noise from a few isolated cases of extremely high TCWV [Muetzelfeldt et al. \(2024\)](#). They also showed that relative humidity (RHmid) is a second promising variable for predicting MCS occurrence, with the probability of such increasing as RHmid increases.

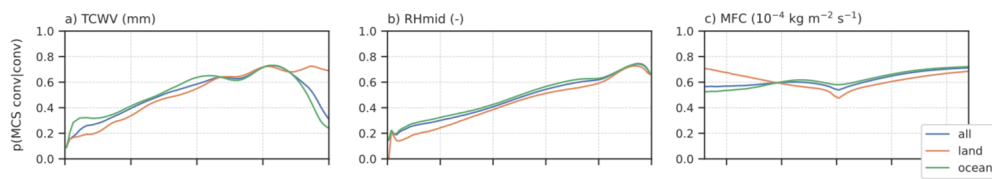


Figure 5: Probability of MCS convection, given the presence of convection. Reproduced from [Muetzelfeldt et al. \(2024\)](#).

RKW theory proposes that the severity of squall lines is strongly related to the tilt of the updraft. Physically, an updraft with a stronger tilt allows for smaller upward acceleration and greater entrainment of environmental air, leading to a weaker, shorter-lived system [Markowski and Richardson \(2010\)](#). Additionally, the theory shows that for optimal longevity, wind shear Δu is exactly equal to the cold pool circulation strength c , $\Delta u = c$, quantified as around 17.25m/s for squall line outflows. A downshear tilting

downdraft occurs where the cold pool is weaker than the shear, but where the cold pool is stronger, the updraft will tilt over the cold pool, with both results leading to a weakening of the system [Markowski and Richardson \(2010\)](#).

1.c *The Main Modes of Variability in the Maritime Continent*

There have been many studies into the diurnal cycle of the Maritime Continent, in particular of precipitation, convection, and surface winds. [Worku et al. \(2019\)](#) used satellite observations to investigate precipitation and convection. They found that precipitation often begins over the islands between 15:00 and 18:00 and continues through the evening, being at its heaviest over areas of high ground, such as mountain ranges. During the day, precipitation over the islands was found to be minimal, but by contrast, precipitation was seen to peak over the ocean at 06:00, particularly near coasts, and decreases again through the day ([Worku et al. \(2019\)](#)).

The diurnal cycle of mesoscale convection was also presented, and was found to follow a similar pattern ([Worku et al. \(2019\)](#)), where here an MCS is defined to be any system found with cold cloud top temperature (CTT) below 250K extending for an area of at least 2000km². In addition to the area requirement, [Worku et al. \(2019\)](#) implemented a further condition where there has to be at least one point within a system's bounds where the CTT is below 225K. They showed that deep convection was most frequent over the islands from early evening until around 03:00 local time, with land-based convection, as with precipitation, generally being less common through daytime hours. Oceanic convection was found to also be confined to coastlines, most frequently to the west of Sumatra [Worku et al. \(2019\)](#). Some of this may be explainable by offshore propagation, a suggestion that is supported by the study by [Lu et al. \(2021\)](#), who investigated 950-850hPa winds over the domain, the result of which is shown in Figure 6. They showed that through late afternoon and into early evening, winds are generally moving towards the islands, consistent with the concept of sea breezes outlined in [Wallace and Hobbs \(2006\)](#). Due to the faster heating of land compared to ocean areas during the day, a feature resembling a density current forms, with cooler air from over the ocean moves towards the land to replace the air rising from over the warmer surface. It was also noted that, during the night, this pattern reverses due to the ocean typically having a slower response to differences in heating [Wallace and Hobbs \(2006\)](#). This explains why, in Figure 6(a), the averaged winds were found to move offshore between 06:00 and 09:00 ([Lu et al., 2021](#)), having clearly changed direction at some point during the night. This offshore wind could be hypothesised to be at least partly responsible for the presence of convective systems just off the coast in the very early morning.

It can be expected that the diurnal cycle of MCSs would look similar to the diurnal

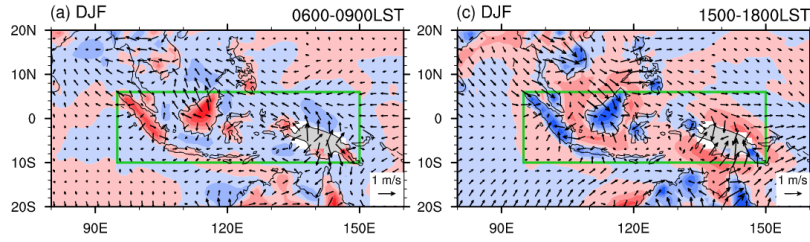


Figure 6: 950-850hPa averaged winds over early morning and late afternoon, reproduced from [Lu et al. \(2021\)](#).

cycle of precipitation, due to previous findings that MCSs are responsible for up to 70% of the precipitation in the Maritime Continent, so a large fraction of the precipitation shown will be as a result of MCSs [Nesbitt et al. \(2006\)](#).

[Chen and Houze Jr \(1997\)](#) considered how deep convection varies over the Tropical Pacific. What they found was similar to the findings of [Lu et al. \(2021\)](#), with deep convection being more prevalent over land during evening hours than morning hours, with the opposite being true for morning hours. It was additionally found by [Mohr and Zipser \(1996\)](#) that the magnitude of the diurnal cycle was stronger over land than over the ocean (varying by around 60% over land as opposed to around 35% over ocean). Whilst similar results can be hypothesised with the Maritime Continent, although it should be noted that the results of [Mohr and Zipser \(1996\)](#) apply to the difference between continental MCS, and those over open ocean.

1.d *MJO*

The Madden-Julian Oscillation (MJO), is characterised by periods of enhanced and suppressed convection. With a period of 30-60 days, the MJO moves from the Indian Ocean, eastwards through the Maritime Continent and into the Pacific [Holton and Hakim \(2013\)](#). Figure 7 shows how the MJO modulates convection in the Tropics [World Climate Service \(2021\)](#). As it passes eastwards through the Maritime Continent, the region will initially clear conditions with little rainfall, as sinking air inhibits convection. This then allows a large increase in surface temperature, which contributes alongside easterly winds to lower level convergence and rising air, which will then bring a period of enhanced convection and precipitation to the region.

[Peatman et al. \(2014\)](#) found that, for the Maritime Continent, phase 1 is generally associated with positive CTT anomalies, which are at their highest towards the centre of the domain over Java, in excess of 10K. The enhanced convection associated with the MJO begins to enter the domain during phase 2, with average CTT decreasing in the west. They found that this region of low CTT then propagates eastwards through the Maritime Continent, with temperatures further decreasing to an anomaly lower than -10K in phase

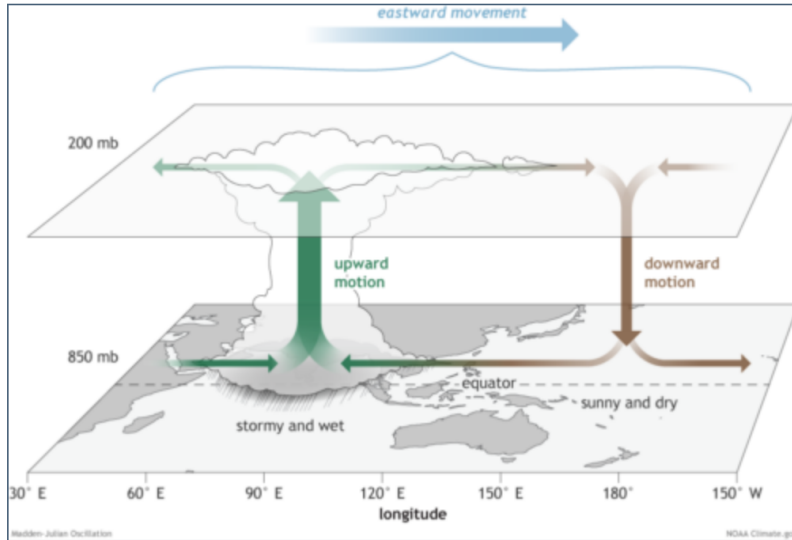


Figure 7: Diagram showing the propagation and characteristics of an MJO event. Wet conditions associated with increased convection approach the Maritime Continent from the west and leave as they enter the Pacific Ocean. Reproduced from [World Climate Service \(2021\)](#)

5, again over Java. Beyond phase 5, the region of low CTT then leaves the domain, once again being replaced by a large negative CTT anomaly ([Peatman et al. \(2014\)](#)).

They also investigated precipitation through different phases of the MJO and found that it follows a similar pattern to CTT, with the strongest positive anomalies, implying a period of enhanced convection, exceeding 5mmhr^{-1} in the central Maritime Continent during phase 5, with the driest phase being phase 1, with negative anomalies of similar magnitudes ([Peatman et al. \(2014\)](#))

1.e *ENSO*

The El Niño Southern Oscillation (ENSO) is indicated by SST anomalies in the east Pacific, and has a period of around 5 years ([Holton and Hakim \(2013\)](#)), although this can vary from 2-7 years. During neutral conditions, schematically shown in Figure 8(a), the Walker Circulation is such that air is generally descending over the east Pacific, resulting in an easterly prevailing wind across the Pacific (trade winds), and ultimately low-level convergence over the Maritime Continent. This causes air to generally rise over the Maritime Continent, and thus frequent occurrences of deep convection.

During El Niño years, positive anomalies in SST are seen in the east Pacific, resulting in increased convection in this region. This is linked to a weakening, or even reversal, of the easterly trade winds ([Wallace and Hobbs \(2006\)](#)), and low-level divergence with generally sinking air over the Maritime Continent.

It is widely agreed that El Niño years are associated with decreased precipitation over

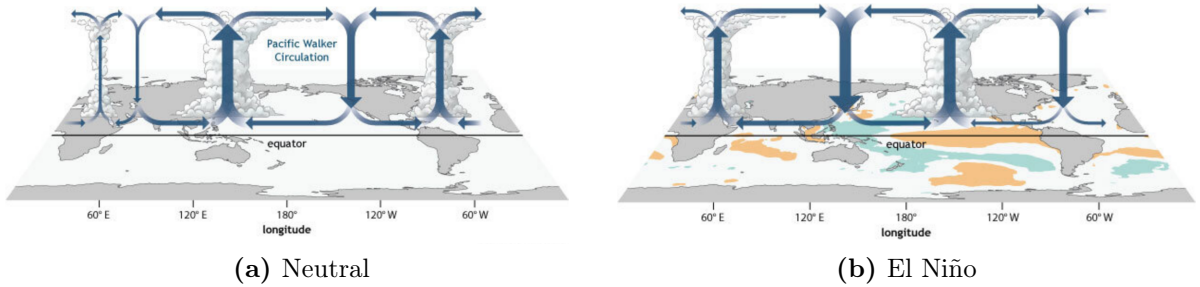


Figure 8: The Walker Circulation during (a) neutral conditions and (b) El Niño conditions. Upward arrows indicate areas of convection, orange areas indicate areas of positive SST anomaly, and blue areas indicate negative SST anomaly. Reproduced from [NOAA \(2014\)](#)

the Maritime Continent ([Wallace and Hobbs \(2006\)](#), [Dai and Wigley \(2000\)](#)), and so it can be hypothesised that El Niño would also result in a decrease in MCS numbers. [Dai and Wigley \(2000\)](#) in particular found that the Maritime Continent was the region most strongly affected by dry conditions during El Niño years, with precipitation being 30-80mm below normal.

Since MCSs account for so much of the precipitation over the Maritime Continent, it is highly probable that at least some of this decrease in precipitation can be explained by a decrease in MCS activity.

Throughout this project, two convection-permitting models are considered, which the distribution and characteristics of MCSs identified by a filtering algorithm compared with each other and with four years of observations data.

2. Data

The period being studied is Boreal winter (December, January, February), with November being run but not used to allow the model to spin up, over 10 years between 2003 and 2018 that encompass a range of ENSO and MJO conditions, and coincide with observations field campaigns.

The data used in this study consists of the output of two atmospheric models, plus available observations.

The first model model is MC12, which parameterises convection over a 12km grid at the equator, although the use of the N2180 grid configuration, the precise grid spacing is 0.140625° zonally, and 0.09375° meridionally. The domain is slightly larger than the one presented in this study, at 20°S - 20°N and 85° - 160°E . The reason for this is that the domain of the explicit model, MC2, is a subset of the MC12 domain, with a 5° buffer on all sides ([Howard et al., 2024](#)).

The second model is MC2, which models convection explicitly on a 2km grid at the equator, or 0.02° in both zonal and meridional directions. The MC2 domain, as outlined previously, is 15°S - 15°N and 90° - 155°E . In the interest of consistency, only this domain is considered in this study (with the outer edges of MC12 removed).

Initial conditions were obtained for both models from ERA5. The boundary conditions for MC12 are also ERA5, however the MC2 is driven by MC12 in that MC12 forms the boundary conditions used by MC2. MC12 also has a slightly longer timestep, at 3 minutes, compared to MC2's timestep of 1 minute.

The models are coupled to a mixed-layer KPP ocean, to which a long timestep can be applied. This allows for the interactions between the ocean and the atmosphere to be shown.

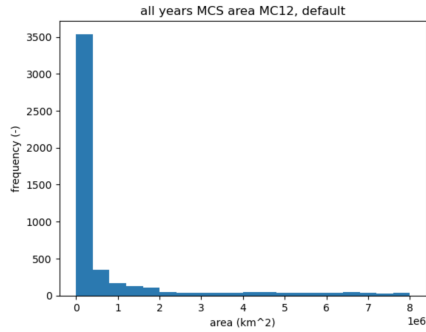
In order to compare the behaviour of the models with previous studies, many of which use observations data, this study also makes use of observations, although it should be noted that this is only available for 2015 onwards. CTT data is Himawari 8 data (available on request from the Japanese Meteorological Society), with a native resolution of 2km, although this is also re-gridded to the MC12 grid. The central wavelength used in this study is 10.4 micrometers, allowing it to pick up high clouds made of small particles. The precipitation data is GPM-IMERG v6, archived on CEDA.

3. Sensitivity to Definitions

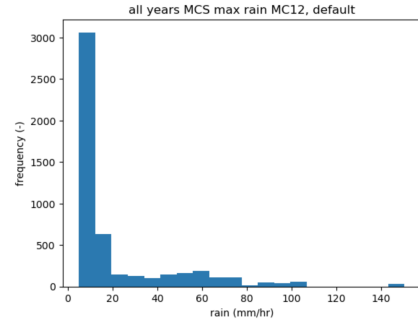
The definition of an MCS according to this study is that there must be a CTT below 250K for an area of at least 2000km², in addition to some convective precipitation exceeding 5mm hr⁻¹, which is similar to that of [Mohr and Zipser \(1996\)](#). However this is not a generally agreed upon definition when considering MCS detection algorithms, and many other studies, such as [Chen and Houze Jr \(1997\)](#), use different definitions. For example, it is not uncommon to use larger areas, such as the 5000km² area threshold used by [Chen and Houze Jr \(1997\)](#). Doing so would mean that it is unlikely that a large system that does not meet the technical definition of an MCS presented in [Markowski and Richardson \(2010\)](#) would be filtered as such. However, this may come at the expense of not filtering MCSs that are relatively small in area, which could particularly affect areas over land, since land-based MCSs are often smaller in area than oceanic MCSs ([Huang et al. \(2018\)](#), [Mohr and Zipser \(1996\)](#)).

Whilst the similarity of MCS definition to that used in [Mohr and Zipser \(1996\)](#) has been chosen due to the similarity in grid size, with the Maritime Continent frequently being shown in their results, two alternative definitions (with a focus on the relationship between the area of the convective core and the total cloud shield area) are presented and considered for MC12, although it should be noted that in all other investigations only the default definition is used. The default only requires precipitation in a single grid cell to exceed 5mm hr⁻¹, which comes with the limitation that there is a chance that a cloud will only be incorrectly classified as an MCS when it is only producing precipitation in one location. The first alternative definition presented considers a convective core that extends for at least 10% of the total cloud area. This would mean that the area occupied by convective precipitation is required to be larger for larger systems. The second considers a set size for the convective core, at 760km².

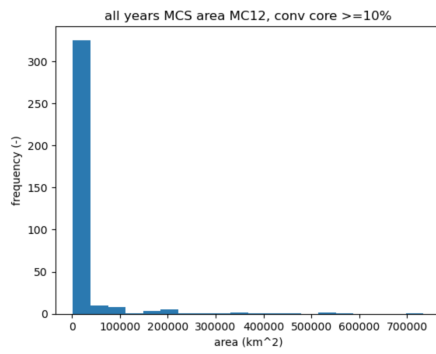
Figure 9 shows the result of plotting histograms of this data. Both area and maximum precipitation area heavily skewed toward lower values. The lowest numbers of MCSs, and the highest skew for area, were detected for the first alternative definition. This may be because, for an MCS to have an area exceeding 100,000km², it would need to contain a convective core of area at least 10,000km², or about $\frac{1}{10}$ the area of Java. Large systems like this are likely to be relatively rare, however the lower skew in the precipitation histogram indicates that rainfall as a result of such systems may be more intense.



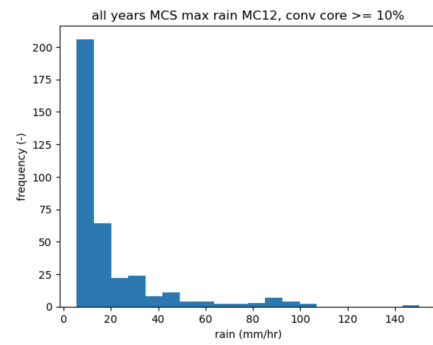
(a) Areas



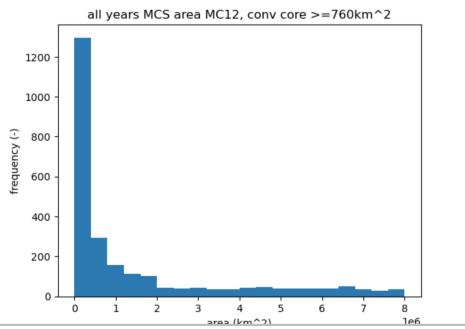
(b) Maximum Precipitation



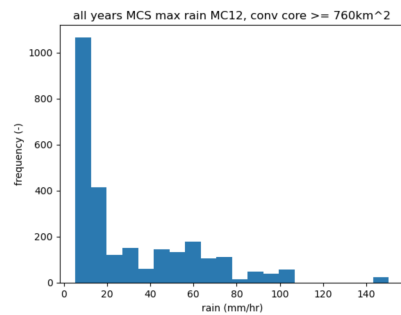
(c) Areas (convective core > 10% cloud area)



(d) Maximum Precipitation (convective core > 10% cloud area)



(e) Areas (convective core > 760km²)



(f) Maximum Precipitation (convective core > 760km²)

Figure 9: Area and maximum precipitation distribution for MC12 MCSs with the definition used in this study (top), convective core exceeding 10% of the total cloud area (middle), and set convective core area of 760km²

4. General Characteristics of MCSs in the Maritime Continent

4.a *Spatial Distribution*

Figure 10 shows the average locations of detected MCSs for the two simulated atmospheres and observations, normalised by

$$\frac{MCSs - min}{max - min}$$

for each of the three sets, where MCSs represents the number of MCSs per season for a given grid point, and min and max represent the minimum and maximum number of MCSs per season in the domain. Doing this allows the three sets to be compared directly.

During the four years of available observations data, MCSs are concentrated over Sumatra and Java, and in the Java Sea. A large number of MCSs were also detected over Borneo and Papua New Guinea. Physically, this is not surprising. MCS occurrences over land can be partly explained by the strong diurnal cycle of heating; over the morning and into the afternoon the temperature of the surface rises quickly, which by conduction heats the lowest layers of the atmosphere, causing air to begin rising. While this heating by itself may sometimes cause sufficient convection for MCS formation, in some locations it is aided by orographic features. The forced lifting over the centre of Papua New Guinea and the west coast of Sumatra may help to explain the relatively large concentrations of observed MCSs in these locations.

The Java Sea, being extremely shallow, exhibits a diurnal cycle of surface temperature stronger than that of open ocean, with surface temperatures frequently nearing 30°C. This, alongside the moisture provided by the sea, aids in the development of large convective systems, hence the large number of MCSs here as well.

MC2 does a generally good job in placing the locations with the highest MCS densities, agreeing with observations that Java and the Java Sea experience the most on average. A notable difference between MC2 and the observations is seen in the island to the immediate east of Borneo. Observations show that MCSs over this island are relative uncommon, however MC2 suggests otherwise, with this island containing some of the highest densities. Modelling the flow around Borneo is complex as it is surrounded by warm, shallow ocean and islands with intricate and varied topography. In particular, the island with the anomalously high MCS density has a lot of very high ground, 1500m (1), so it could be argued that MC2 may be too sensitive to the interactions between topography and flow, leading to unrealistic results. On the other hand, MCS densities for MC2 are much lower than observations over the mountain ridge in Papua New Guinea. It's possible that MC2's lack of sensitivity here, even though much of the topography is over 3000m, is due

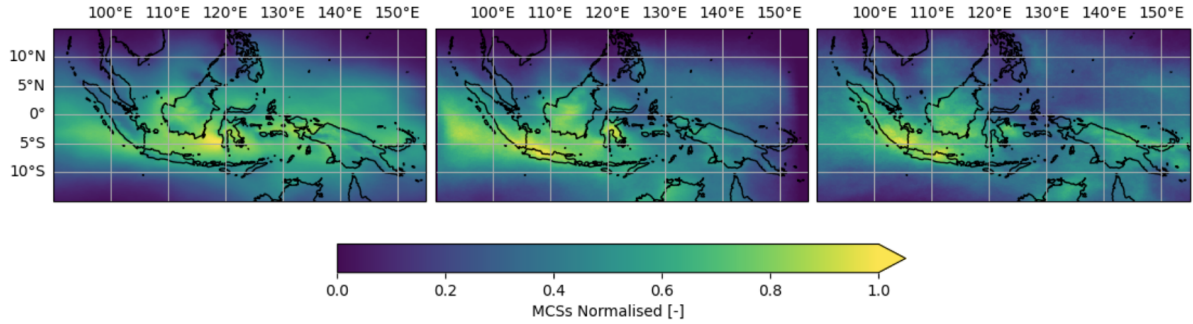


Figure 10: Average MCS locations for MC12 (left), MC2 (middle) and observations (right), normalised

to the more consistent prevailing winds, as a result of the open ocean to the north.

By contrast, MC12 for the most part places MCSs evenly throughout the centre of the domain, with a particular area of high MCS density to the immediate south-east of Borneo.

These results differ from those found by [Huang et al. \(2018\)](#), who showed a much higher concentration over the islands than the ocean. A possible reason for this is that they used a CTT threshold of 233K, as opposed to 250K in this study. In addition, the area over which the low CTTs must be maintained is much larger, at 5000km². [Huang et al. \(2018\)](#) also noted that MCSs over land tend to be more intense, where intensity in their study is defined by particularly low CTT. It's possible then that oceanic systems, which on average have a higher CTT than their land-based counterparts, are being filtered by the algorithm in this study as their CTT is still below 250K, but wouldn't be by [Huang et al. \(2018\)](#).

[Mohr and Zipser \(1996\)](#), on the other hand, uses a similar MCS definition, on a similar grid. They also found a multitude of MCSs over the ocean, particularly over the Java Sea. However, the concentration of MCSs over the southern tip of Papua New Guinea in their study noticeably exceeds that of the observations in this study. It is likely that this is due to the timing of observations made by [Mohr and Zipser \(1996\)](#). At 18:00 local time, many studies into the diurnal cycle of deep convection ([Chen and Houze Jr \(1997\)](#), [Worku et al. \(2019\)](#)) find there is a large concentration of precipitation and convective systems at this time. The observations presented in Figure 10 are averaged over 00:00, 06:00, 12:00 and 18:00, with land-based MCSs being found to be relatively uncommon until the mid-afternoon ([Huang et al. \(2018\)](#)). Given this, it would be expected that MCS density over these regions is lower than presented in other studies.

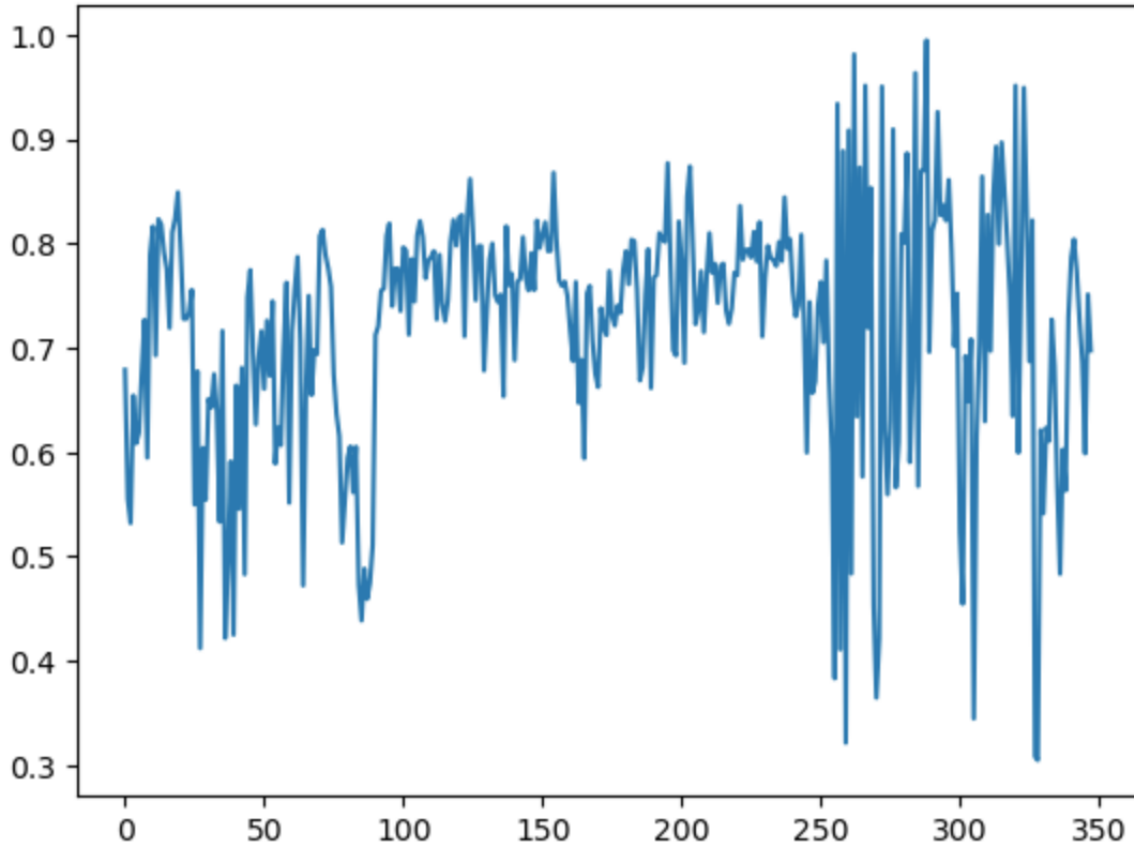


Figure 11: Fraction of precipitation accounted for by MCSs

4.b *Fraction of Precipitation Associated with MCSs*

It has been previously established that the fraction of precipitation associated with MCSs in the Maritime Continent (and the tropics in general) is expected to be over 0.5 [Nesbitt et al. \(2006\)](#). Figure 11, generated by dividing the sum of precipitation within MCS boundaries by total precipitation within the domain, supports this for the most part. It can be argued that the fraction found by this study is slightly too high, however this is likely to the low cloud shield area and convective precipitation thresholds, compared to other studies. It is noted that the periods towards the start and end of the observation period display higher variability in MCS precipitation fraction than the middle years. These highly variable years coincide with El Niño years, however conclusions on whether El Niño conditions lead to an increase in variability cannot be drawn at this time, due to the limited number of years in the observations dataset.

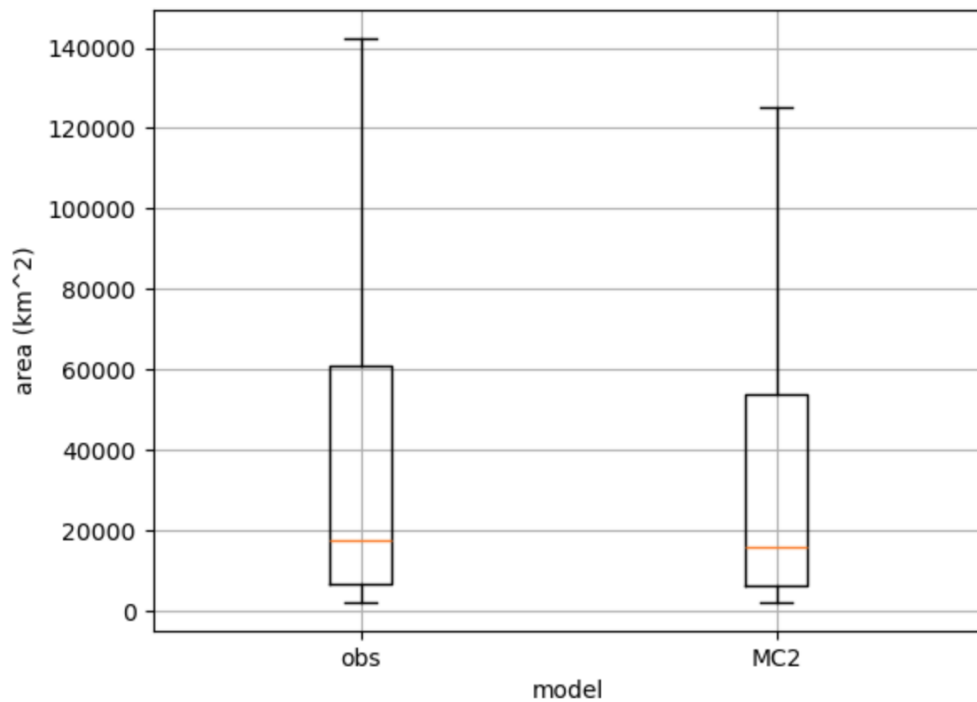


Figure 12: Distribution of MCS areas from MC2 compared to those of observations

4.c *Area and Maximum Precipitation*

Throughout this study, the characteristics of MCSs produced by MC2 and MC12 are shown to substantially differ from each other. The area of MCSs produced by MC2 are generally close to the area of observed MCSs (as shown in Figure 12), however MC12 often produces MCSs that are fewer in number, but an order of magnitude too large. Both simulations frequently overestimate precipitation.

5. Diurnal Cycle

5.a *Diurnal Cycle Methods*

In light of the investigation by [Mohr and Zipser \(1996\)](#), it could be reasonable to hypothesise that MCSs in the Maritime Continent may exhibit their own diurnal cycle, though their numbers and characteristics may differ from global MCSs. For instance, much of the ocean surrounding the islands is extremely shallow, leading to sea surface temperatures (SST) exhibiting a stronger diurnal cycle than those in open ocean would. This could lead to the diurnal cycle of MCSs in the Maritime Continent more closely resembling that of the land-based MCSs, despite much of the area being oceanic.

For each day where MC2 and MC12 data are available, the number of identified MCSs in the domain at each hour is counted using CTT and precipitation data as outlined previously. The mean number of MCSs in the Maritime Continent at each hour is then obtained through summing the detected MCSs across each year, before dividing this total by the number of days in the set.

This process is repeated for available observations data, although it should be noted that only four years of observations data are available.

Given the findings of [Mohr and Zipser \(1996\)](#), we also separate MCSs into a land-based and oceanic group, so that any differences between MCS diurnal cycles over land and over ocean can be seen. To perform this, a land mask is applied to the domain, separating areas of land from areas of ocean. MCSs are then split into a land group and an ocean group, depending on the location of their centroid. It can be hypothesised that, as with diurnal cycles of surface temperature and precipitation, MCS numbers would vary more substantially over land than over ocean.

Diurnal variations in MCS numbers may be largely explainable by variability of the main drivers of convection, such as SST, surface temperature over the land, and specific humidity. Where this is applicable, these variables are extracted and their diurnal cycle is averaged as with MCS numbers.

In addition to MCS numbers being found by previous studies to vary diurnally, [Huang et al. \(2018\)](#) also noted that their intensity undergoes a diurnal cycle of its own. They found that land-based MCSs were more intense than oceanic MCSs. This supports the idea that MCS activity is heavily influenced by at least some of the driving factors outlined in the previous section, with surface temperatures over land being higher during the day, and with many areas above 1,000m in altitude, it can also be hypothesised that there may be some orographic influence of MCS activity.

Two proxies for MCS intensity are proposed for this study. The first is the area of the cloud shield; an MCS covering a larger area may indicate stronger convection, and

have an impact on a larger proportion of the population of the islands. The second is the maximum precipitation recorded within an MCS’s boundary, with heavier rain likely to have originated from systems with stronger convection. Over the study period, at local times 00:00, 06:00, 12:00 and 18:00, all data on MCS area and maximum associated precipitation is additionally gathered. Comparisons are then made to [Huang et al. \(2018\)](#), although it should be noted that the definition of intensity used in this study is dependent on CTT, not area and maximum precipitation.

Examining the way the spatial distributions of MCSs change at key times through the day will not only increase confidence in the results of decomposing the MCS numbers into a land and ocean mean, but may help to explain unexpected results that are not captured in the diurnal cycles of any environmental variables. One notable example of a feature within the domain that may locally influence MCS numbers that may not be visible in environmental plots is that of orography. For example, the forced lifting associated with mountainous regions may cause an increased number of land-based MCSs at times that may not be expected within the observed set, as seen in previous studies into MCS diurnal cycles, such as [Mohr and Zipser \(1996\)](#) and [Huang et al. \(2018\)](#).

Four times are identified at equal intervals throughout the day: 00:00, 06:00, 12:00 and 18:00, to allow for investigations into the spatial distributions of MCSs during the middle of the night, the middle of the day, the morning, and the evening. For each season, the number of times a particular grid point is within the bounds of an identified MCS is recorded and averaged over the number of seasons, making the units of the MCS density MCSs per season, unless otherwise specified.

5.b *Diurnal Cycle Results and Analysis*

The average number of identified MCSs in the domain across all days in the set for each simulated atmosphere, plus available observations, are shown in [13](#). Each shows two clear peaks in MCS frequency, with troughs where activity is not as prevalent in between. Given the findings of [Huang et al. \(2018\)](#) it is likely that these correspond to an ocean peak through the early hours of the morning, and a land peak in the afternoon and into the evening. In later analysis we investigate this using a land mask to split oceanic systems from land-based systems. In general, the explicit convection simulation MC2 uses leads to greater numbers of MCSs in the domain than the parameterised convection simulation MC12 uses, with numbers peaking at just under 40 MCSs on average at 15:00 for MC2 and observations. By contrast MC12 MCS numbers peak at 9.5 at just before 05:00 and 20:00.

There is an observed trough in MCS activity from just after sunrise until early afternoon, when the land-based systems start initiating in significant numbers. This feature

is common to both the observations and MC2, however is much less prominent in MC2. It could be speculated that this is because MC2 produces longer-lived systems than are observed, however as the MCS filtering algorithm does not have tracking capabilities, this is beyond the scope of this investigation. For MC12, this trough occurs much later, between mid morning and mid afternoon, with the relative magnitude of the decrease in activity being similar to that in the observations.

Both the observations and MC2 show a second peak from around 15:00 into early evening, which is consistent with the findings of [Huang et al. \(2018\)](#), who showed a peak in land-based MCSs at this time. The second peak for MC2 is around 10% larger than the first, while for observations there is no substantial difference in the magnitude of the two peaks. Investigations into land-based MCSs separated from oceanic MCSs could provide insight into why this occurs.

The timing of the second peak is similar between MC2 and observations, occurring during mid afternoon, but the second peak in MC12 occurs much later, at 20:00. Despite this, its size in relation to the first peak in MC12 is similar to that of the observations, with there being no substantial difference.

Additionally, the largest peak for MC2 is 35% larger than the deepest trough, with the same range in mean MCS numbers being reflected by the observations and MC12. This implies that, despite the differing numbers of MCSs being produced by the two simulated atmospheres, the magnitude of the diurnal cycle for both is consistent with observations.

Similarly to MCS numbers, MCS intensity, as defined in this study, was also found to exhibit a diurnal cycle. The variation in MCS area at 00:00, 06:00, 12:00 and 18:00 is shown in [14](#). It should be noted that in the interest of figure clarity, outliers have been removed, where an outlier is defined as any area value below $LQ - 1.5IQR$, or exceeding $UQ + 1.5IQR$, where LQ is the lower quartile, UQ is the upper quartile, and IQR is the inter-quartile range.

All MCSs identified by [Mohr and Zipser \(1996\)](#) at sunset and sunrise were below $200,000\text{km}^2$ in area, with [Huang et al. \(2018\)](#) finding that the larger oceanic MCS numbers peak in the early morning. Given that the UQ for MC2 at 06:00 does not exceed $200,000\text{km}^2$, it is mostly consistent with the findings of [Mohr and Zipser \(1996\)](#), however a some MCSs were being located with areas up to $450,000\text{km}^2$, suggesting that MC2 may on occasion produce systems of organised convection that are uncharacteristically large for the Maritime Continent. The median for all four recorded times lying well within the range of areas found by [Mohr and Zipser \(1996\)](#), however, is a strong indication that MC2 is generally good at producing MCSs of physically reasonable sizes. However, [Mohr and Zipser \(1996\)](#) concluded that MCSs within the latitudes of the Maritime Continent

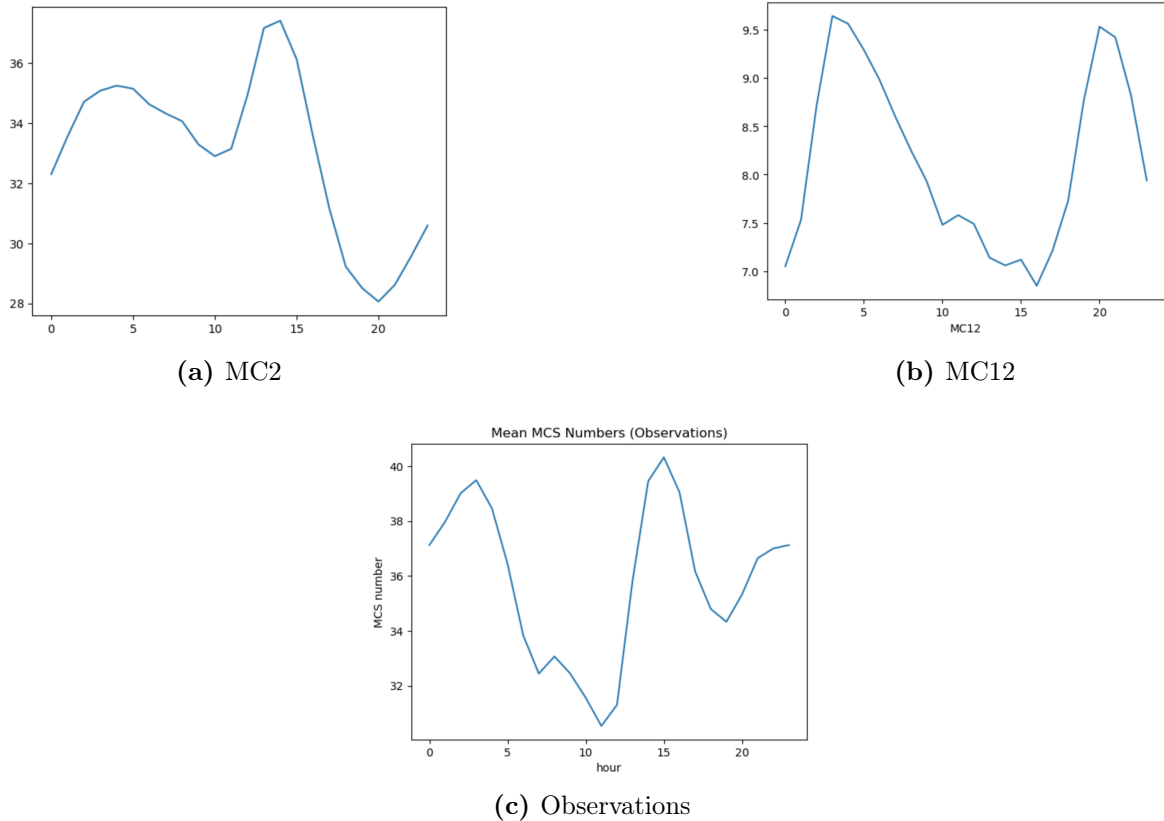


Figure 13: Diurnal cycle of domain MCS numbers, with the hour (local time) on the x-axis, and the mean MCS number at that hour on the y-axis. MC2 and MC12 span the 10 years in the data set, and observations span the last four years, where observations are available. Note the different scales between observations and MC2, and MC12, and that the y-axis does not start from 0.

can generally be expected to have a greater area in the morning than in the evening, and MC2 is inconsistent with this, with many of the largest MCSs identified being those at 18:00, having increased steadily throughout the day.

MC12 does show a diurnal cycle of area consistent with that found by [Mohr and Zipser \(1996\)](#), with maximum MCS areas being found at 06:00. However, MC12 does a poor job producing instances of organised convection with reasonable areas. While the large skew towards the lower areas indicates a majority were of physically reasonable size, the largest identified MCSs in this case are a full order of magnitude larger than would be expected for the Maritime Continent if MCS behaviour during the years included in the data set were to be consistent with those in previous studies, suggesting that the cloud cover produced by the parameterised scheme is too large.

The observed MCSs were the smallest group, with an upper quartile between $50,000km^2$ and $75,000km^2$. Despite this, and the similar grid and MCS definitions, these results are

not consistent with those of [Mohr and Zipser \(1996\)](#), who found the UQ for MCS area in the Maritime Continent should lie between $6,000\text{km}^2$ and $10,000\text{km}^2$. This is due to the fact that the satellite used by [Mohr and Zipser \(1996\)](#) uses a lower frequency, giving it the ability to detect larger droplets and convective cores. The satellite used in this study, with a higher frequency, is able to pick up small particles, such as ice crystals in the outer edges of an anvil cloud, thus larger overall areas are generally found.

The oceanic MCSs being more common than land-based MCSs at 06:00 and 12:00, with these times also containing the largest observed MCSs is consistent with the finding of [Huang et al. \(2018\)](#) that oceanic MCSs are generally larger, however there is no substantial difference between MCS areas at 06:00 and 18:00, an inconsistency with [Mohr and Zipser \(1996\)](#). This may be due to the region of the Maritime Continent itself, which contains large areas of shallow ocean, and may show oceanic Maritime Continent MCSs behaving in ways more similar to the land-based MCSs than the oceanic MCSs in the study of [Mohr and Zipser \(1996\)](#), which would mostly be located over open ocean. In order to investigate the similarities between the characteristics of oceanic MCSs in the Maritime Continent, and those over open ocean, plots similar to those in [Figure 16](#) could be generated, showing MCS area, rather than the number of MCSs in a season.

Whilst the diurnal cycle of maximum precipitation was not explicitly mentioned by [Mohr and Zipser \(1996\)](#) or [Huang et al. \(2018\)](#), the latter did note that oceanic MCSs globally reached a peak in intensity in the morning, around the same time as the peak in area is observed. The observed maximum precipitation is consistent with this, showing that, for the intensity proxy proposed in this study, there is a peak in the early morning. However, [Huang et al. \(2018\)](#)'s conclusion regarding MCS intensity was that the land-based MCSs are more intense, and that these primarily occur later in the day, and so one might expect the diurnal cycle of MCSs in the Maritime Continent to more closely follow this pattern, rather than just that of oceanic MCSs. It is possible that this discrepancy is due to differing definitions of MCS intensity. While maximum precipitation is considered here, [Huang et al. \(2018\)](#) use mean cloud top temperature as a measure of intensity.

Neither MC2 nor MC12 produce a diurnal cycle for maximum precipitation that is consistent with observations, as shown in [15](#). MC2 frequently produces values of maximum precipitation that are too high, albeit of the same order of magnitude, than the observations, with the median MC2 maximum precipitation typically being 33% higher than observed values. The maximum spread for MC2 occurs at midnight, with an IQR of 30mm hr^{-1} . This is 36% higher than the IQR for 12:00, where the lowest spread is found for MC2. On the other hand, the IQR at 06:00 for the observations is 47% higher than that of 12:00, indicating that whilst MC2 does not correctly determine the time at which the MCSs with the largest areas occur, it does a reasonably good job with the magnitude

of the variability.

The diurnal cycle of maximum MCS precipitation produced by MC12 bears few similarities to observations. The average maximum precipitation given by observations is around 10mm hr^{-1} for each time, and MC12 does do this well, however the upper quartile of MC12 being well in excess of the upper quartile for observations indicates that there are a significant number of MCSs with values of maximum precipitation that are too high for the 00:00 results to be consistent with observations.

Over daytime hours, maximum precipitation from MCSs as identified from MC12 decreases. Where the observations show that by 06:00, there is increased spread, perhaps owing to a relatively small number of systems producing very large amounts of precipitation, MC12 shows a decrease in variability, with the vast majority of MCSs at this time producing less than 20mm hr^{-1} of precipitation at their maximum. A similar pattern in the MC12 data is repeated at 12:00, with the difference between MC12 and the observations being even more pronounced, with the maximum value for the maximum precipitation can take without being considered an outlier in the MC12 set being just over one third the equivalent value in the observations.

This contrasts with a sudden increase in maximum precipitation variability at 18:00, where the maximum value identified from the MC12 set without being an outlier being over twice the equivalent observation value. The IQR at 18:00 is also 8 times that at 12:00. Such a substantial increase lends credence to the suggestion that MC12 cannot capture the diurnal variability of maximum MCS precipitation.

These results suggest that MC2 may be better at reproducing the magnitude of diurnal variations in maximum precipitation associated with MCSs, although MC2 may have a bias towards higher values. While MC12 is generally good at determining average value of maximum associated precipitation, it shows a pattern that is not only too large, but is also not how MCSs are observed to behave.

The observations showing that maximum precipitation peaks at 06:00, rather than 18:00 when land-based systems have initiated is in seeming disagreement with [Huang et al. \(2018\)](#), who showed that the land-based MCSs are generally more intense. This discrepancy could be due to differing proxies for MCS intensity, with low cloud top temperature being used more frequently than maximum precipitation. To investigate this, the distribution of this alternative MCS intensity proxy, perhaps alongside mean precipitation in place of maximum precipitation, could be plotted and compared with that of maximum precipitation, and the findings of [Huang et al. \(2018\)](#).

The spatial distributions of MCSs at 00:00, 06:00, 12:00 and 18:00, using the MC2 set, are shown in [16](#) (middle). In general, the results are consistent with previous studies into MCS diurnal variation.

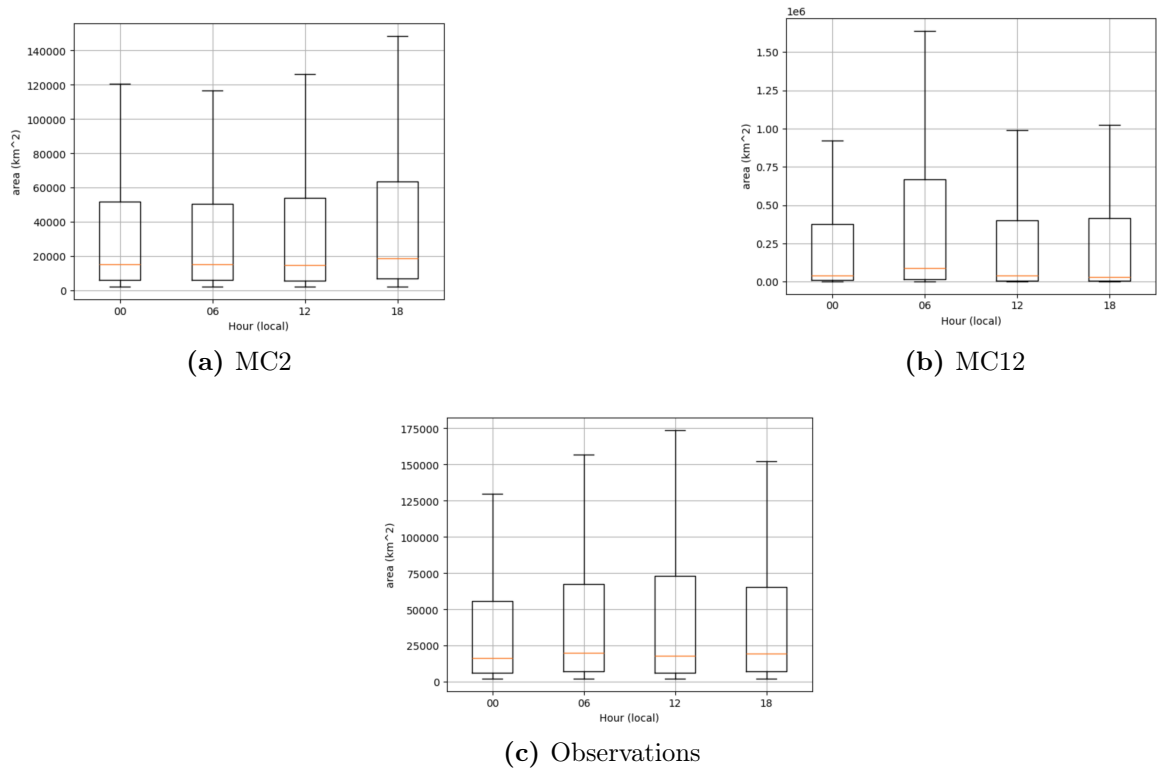


Figure 14: Diurnal cycle of MCS area

At midnight, oceanic MCSs are very infrequent, while there is still some MCS activity over land, particularly in areas near mountains. These systems likely developed over the late afternoon and evening and have not yet dissipated.

By 6am, there is a substantial increase in MCS numbers over the ocean, as was found by [Mohr and Zipser \(1996\)](#). While there is activity over open ocean, much of it is concentrated in areas close to the islands, where the water is shallow. This implies that the diurnal cycle of oceanic MCSs in this region, despite the underlying ocean exhibiting a stronger diurnal cycle in SST than in more open regions, still to an extent display the characteristics of oceanic MCSs in previous studies. In general MCS activity over land at this time is minimal, coinciding with low surface temperatures, further supporting the idea that the diurnal cycle of MCSs in the Maritime Continent shares many characteristics with global MCS populations. However, there is one region of very high MCS density near the centre of Borneo, which does not fit with the expected diurnal cycle. The density of around 45 indicates that, for an average season, the grid points in that area are within an MCS boundary at 06:00 on about half of the days. To the north of this anomalously high region is Mount Kelam, a mountain with a peak of just over 1000m. It is possible that this could be due to MC2 being overly sensitive to the orography, however it is also noted that the same effect is not observed in Papua New Guinea, which contains a mountainous ridge

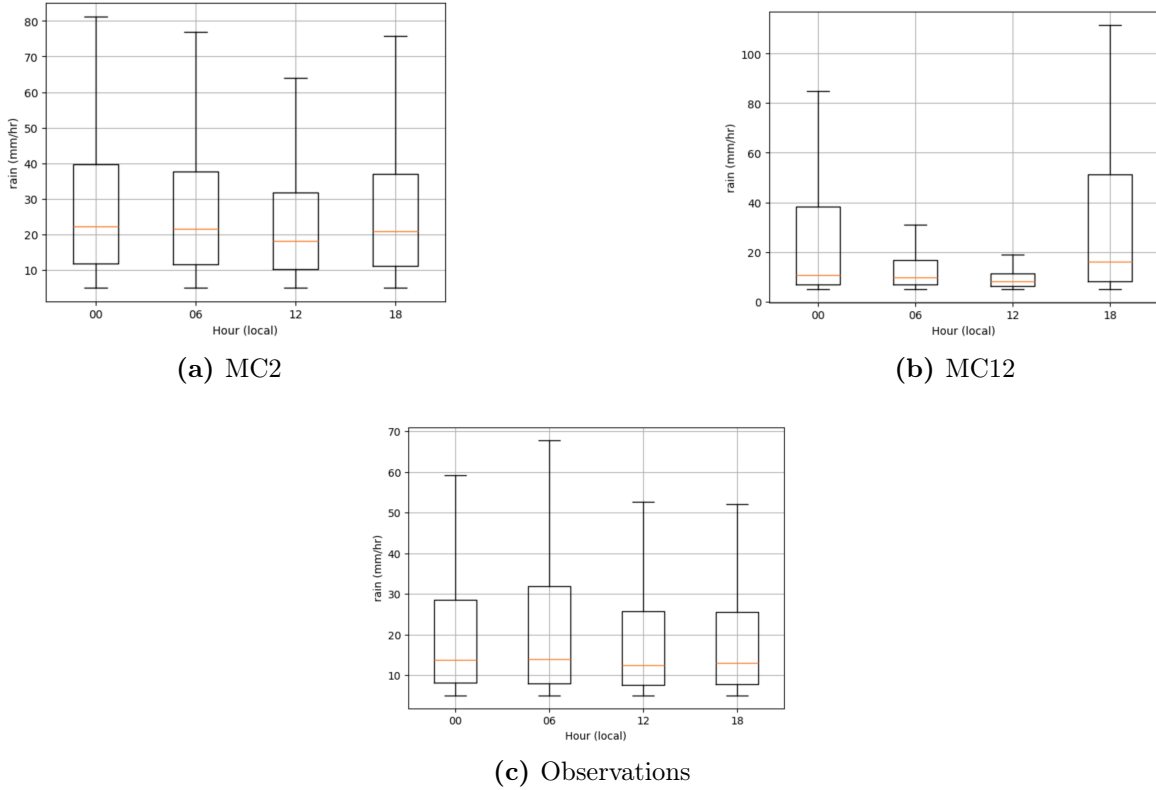


Figure 15: Diurnal cycle of MCS maximum precipitation

with many peaks taller than that of Mount Kelam.

The midday plot shows that MCS activity over land is once again reduced, with many areas displaying a normalised density of 0.06-0.12, or experiencing an MCS at midday on 6%-12% of the days in a given season. The peak in Borneo has additionally decreased to a value more consistent with previous studies. In contrast, oceanic MCS activity is still relatively high, again with many of these systems being found over the warmest water near the islands. This was not discussed in [Mohr and Zipser \(1996\)](#), whose investigation only covered sunset and sunrise due to the fact that the satellite observations used are only available at this time, but is not entirely unexpected given the mean MCS number by hour plot for MC2 in the previous section, which showed activity beginning to increase for the second time at around midday.

Towards the evening, oceanic MCSs begin to dissipate, whereas land-based systems are starting to initiate in significant numbers. These land-based MCSs are most prevalent in areas with a lot of high ground, particularly along the mountainous ridge in Papua New Guinea. Physically this could be explained as a result of the forced lifting associated with this orography making the LFC more reachable for a given parcel of rising air. Alternatively, or perhaps additionally, the particularly strong peak over mountains could indicate that MC2 is overly sensitive to orography, particularly when considered alongside

the 6am Borneo peak. Comparisons with observations will indicate whether or not the magnitude of this effect, compared to other areas of land, is unrealistic.

Figure 16 (top) shows the same plot as in 16 (middle), but using MC12 instead of MC2. Figure 13 showed two peaks in MC12 MCS activity, likely corresponding to a land peak and an ocean peak, however the parameterised convection scheme did a poor job establishing the timing of these peaks compared to MC2. 16 gives some insight into whether MC12's placement of MCSs is physically realistic.

At midnight, substantial MCS activity occurs over both land and ocean, particularly over mountainous areas and warm water. Whilst observations do show MCS activity over land and some evidence of systems drifting over ocean at this time, large numbers of oceanic MCSs would not be expected, and so MC2's placement of the activity that does occur is more physical, even if its frequency is slightly too low over the ocean directly over the ocean surrounding Papua New Guinea.

A large majority of MCSs occurring at 6am are oceanic, which is in agreement with [Mohr and Zipser \(1996\)](#). Additionally, the activity occurring Mount Kelam, whilst still larger than most land areas, is not as substantial, which suggests that MC2 may have been interacting with the flow and orography in an unrealistic way.

At midday, there is an overall trough in activity everywhere, coinciding with expectations. The area with the most activity at this time is the extremely shallow ocean just South-East of Borneo, likely aided by the high SSTs.

By 6pm, activity overall has just begun to increase again, a result that differs greatly from both MC2 and from available observations, showing a peak in MCS activity over mid-afternoon and into the evening. MC12 also does not show as strong a peak over the mountains in Papua New Guinea as MC2 does, indicating that at least one of these simulated atmospheres does not show MCSs behaving as they do in the Maritime Continent.

The observed MCSs in the region follow a similar cycle, and are in agreement with the investigation into convection over the tropical Pacific by [Chen and Houze Jr \(1997\)](#), who showed that instances of severe convection in the Maritime Continent are generally more common over the ocean during the morning and until mid afternoon, with systems over land initiating later in the day and into the evening.

Comparing the 18:00 and 00:00 distributions shows some evidence of offshore propagation through the evening. Areas of land have a much stronger diurnal cycle than areas of ocean, particularly that of open ocean, due to the land having a much lower heat capacity. Then, during the morning, the surface temperature of the land increases faster than the SST, resulting in the difference between land and sea surface temperature increasing. When this difference reaches 5° , rising air over the land allows the cooler air over the ocean to move towards the coast, resulting in a sea breeze [Wallace and Hobbs \(2006\)](#).

After sunset, the land cools faster than the ocean, with SST now generally warmer than land surface temperatures. This causes the density current outlined above to reverse, with the flow now moving offshore, turning the sea breeze into a land breeze [Wallace and Hobbs \(2006\)](#). MCSs can be carried offshore on this breeze, resulting in the population of oceanic MCSs around the coastal seas in the 00:00 plot.

As is the case for environmental variables such as surface temperature, the diurnal cycle of observed MCSs is visually weaker for oceanic systems than with those initiating over land. One oceanic location exhibiting a strong diurnal cycle is the ocean south of Borneo, a feature which was also seen for the two atmospheres. As outlined previously, this is due to shallow depth of this sea causing a much stronger diurnal cycle in SST than would be observed in other oceanic parts of the domain.

[Chen and Houze Jr \(1997\)](#) shows that many land-based systems initiate over or near areas with mountains, where air is forced upwards and it is more likely the LFC will be reached. A similar pattern is seen in the observations, with the mountain rides through the centre of Papua New Guinea, and near the west coast of Sumatra, showing areas of particularly elevated MCS activity compared with most other areas of the domain.

MC2 has a strong peak in MCS activity in Borneo at 06:00, with MC12 showing a similar signal at this time, although since the 00:00 distribution shows a much larger peak in this location for MC12, it is likely that this is explainable by long-lived, land-based systems that have not yet dissipated. Borneo does not display observed enhanced MCS activity at 06:00. One possible explanation for the increase overnight in Borneo in MC2 is in the interactions between orography and the flow in the domain. To the south of Sumatra and Java, and to the north of Papua New Guinea, is open ocean, leading to consistent prevailing winds. The flow around Borneo is much more complex, with it being surrounded on all sides with warm ocean and islands with varied topography, which could perhaps lead to some unrealistic effects.

Figure 17 shows the result of separating land-based and oceanic MCSs and plotting their diurnal cycles. Considering the study of [Huang et al. \(2018\)](#) it could be expected that the diurnal cycles of the two groups would follow similar patterns, but be offset such that the peak in numbers of oceanic MCSs would be in the early morning, with the peak for land-based systems being much later, in the afternoon. The observations show that the magnitudes of the land-based and oceanic diurnal cycles are similar, with the number of land-based MCSs at 10:00 local time being 70% that at 15:00, and the number of oceanic MCSs at 10:00 being 80% that at 15:00. This would make sense given the shallow Java Sea exhibits a large diurnal cycle of SST, relative to regions of open water.

In agreement with [Huang et al. \(2018\)](#) there is a prominent peak in observed oceanic system numbers in the early morning, while the land-based systems peak in number in

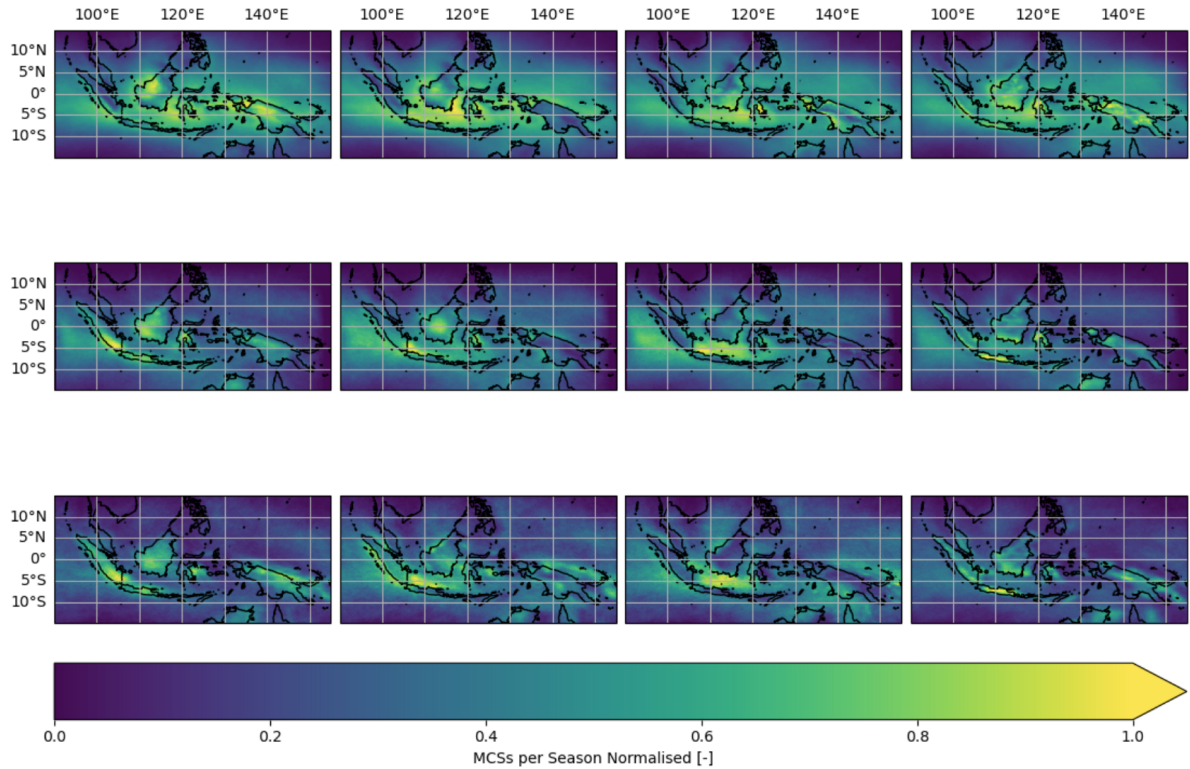
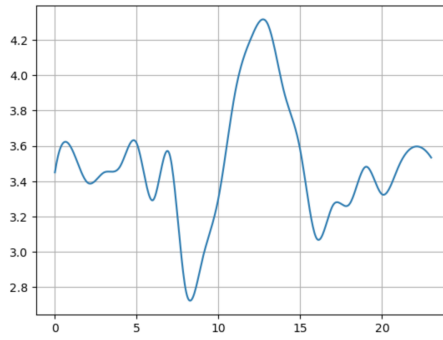


Figure 16: Spatial distribution of MCSs at 00:00 (left), 06:00 (middle left), 12:00 (middle right) and 18:00 (right), for MC12 (top), MC2 (middle) (both over 10 years), and available observations (bottom) (over 4 years)

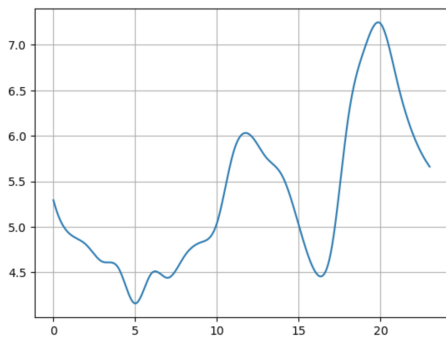
the mid afternoon. There is an additional secondary peak in both profiles, signaling a relatively large number of MCSs over land while oceanic MCSs reach their main peak, and vice versa in the afternoon. At least some of the oceanic MCSs contributing to the increase in number through the evening are likely to be those that initiate over land and drift offshore on a land breeze, some evidence of which can be seen in Figure 16.

By contrast, neither MC12 or MC2 agree with previous studies. Whilst the timing of MC2’s land peak occurs just before 15:00, and its magnitude matches observations, the diurnal cycle of land-based and oceanic MCSs is virtually identical. As previously outlined, some similarities in the behaviour of oceanic and land-based MCSs in the Maritime Continent is not unexpected due to how shallow the Java Sea is. However, since MC2’s oceanic MCSs do not resemble that of the observations, it is likely that MC2 is too sensitive to varying SSTs, particularly over the Java Sea.

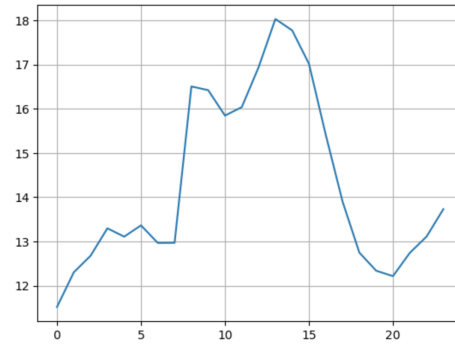
MC12 does a poor job determining the timing of peak MCS activity, with numbers over land being too low and peaking too early. Whilst observations and MC12 showed MCS numbers increasing later in the day, the early morning peak in oceanic activity found by Huang et al. (2018) was not seen in MC12.



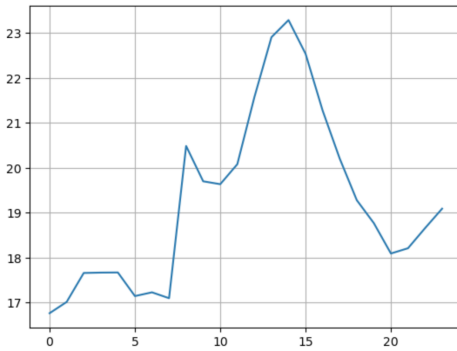
(a) land, MC12



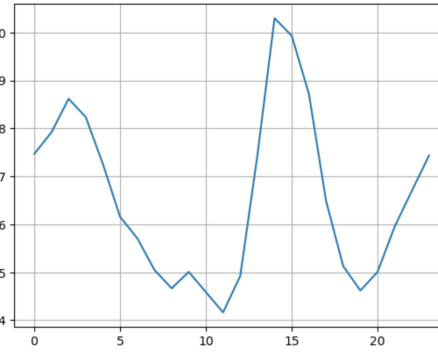
(b) ocean, MC12



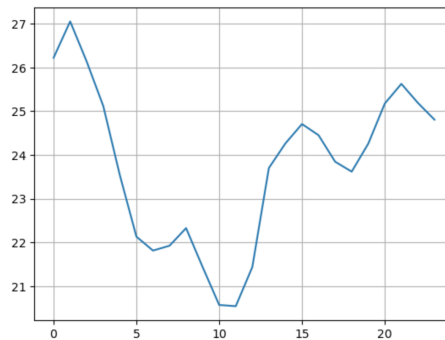
(c) land, MC2



(d) ocean, MC2



(e) land, observations



(f) ocean, observations

Figure 17: Diurnal cycle of MCS numbers according to MC12 (a,b), MC2 (c,d) and observations (e,f) with land-based and oceanic separated

6. The Madden-Julian Oscillation (MJO)

6.a *MJO Methods*

The MJO has a strong effect on precipitation in the Maritime Continent ([Peatman et al. \(2014\)](#)), but its specific effect on MCSs in this region is not fully known, although some studies into broader regions have been conducted. For example, [Hendon and Liebmann \(1994\)](#) found that there was a substantial increase in mesoscale convection, with the maximum variance (up to 4 times in enhanced MJO phases) occurring over the Indian Ocean. It is likely that a similar pattern will be demonstrated, with activity going through periods of enhanced and suppressed convection, moving from west to east. To investigate this, MCS data is separated by phase. Over the Maritime Continent, during phases 1 and 2 the area of enhanced convection is over the west side of the domain, by phases 3 and 4 this has moved over the centre of the Maritime Continent, and by phases 5, 6, 7 and 8 the enhanced convection moves to the east and out of the domain.

Information on dates, MJO phase and amplitude is available from the Australia Bureau of Meteorology. Until 2014, outgoing longwave radiation (OLR) and tropospheric winds were used to locate areas of enhanced convection as in [Wheeler and Hendon \(2004\)](#). However, it was later determined that the methodology of [Wheeler and Hendon \(2004\)](#) unnecessarily removed ENSO variability, so the method used by the Bureau of Meteorology moved to that proposed by [Gottschalck et al. \(2010\)](#). This dataset is filtered such that it only contains dates for which MCS data for MC12 and MC2 is available. The phases are then separated from each other, with their dates recorded. Phase 0, defined here where the amplitude of the MJO < 1 , where MJO activity is weak, is additionally separated and is used as a benchmark to compare activity in other phases, and thus identify phases with enhanced and suppressed convection.

For each of the phases, CTT and precipitation data for each date are used as input for the MCS detection algorithm. The number of MCSs and their spatial distribution, is recorded, as are their areas and maximum associated precipitation.

Presenting this data could lead to some misleading results, as if a longer period of time had been spent in a given phase, the number of MCSs in that phase would be naturally high. Instead, the total number of MCSs in each phase, and their spatial distributions, are divided by the number of days in that phase to give a relative frequency that is not dependent on the length of time spent in a phase.

The relative number of MCSs in each phase is then displayed in a bar graph, with phase 0 providing a benchmark with which any enhanced or suppressed periods of MCS convection can be determined. This is then compared with previous studies into MCSs within a broader region, and convection in general in the Maritime Continent.

As a result of the methods outlined above, the MCS distribution data is now in units of MCSs per day. To calculate the anomaly each phase results in, the mean must also be converted to the same unit. By default it is in MCSs per season, and so each value is divided by 90 (the length of the season in days). From here the anomaly is then calculated by

$$anomaly[phase] = MCSs[phase] - mean.$$

Each anomaly is then plotted over the domain, with regions of red corresponding to areas of greater activity than mean, and regions of blue being areas of less activity than the mean. Much like the investigations into the diurnal cycle, MCS areas and maximum precipitation are separated by MJO phase and shown in a box plot. This allows for discussion of whether, in addition to any effects on MCS numbers, the MJO has any notable influence on their intensity as defined in this study.

6.b *MJO Results and Analysis*

Plotting the relative frequency of MCSs separated by MJO phase, for each simulation and observations, results in the plot shown in Figure 18. The red bar corresponds to phase 0. Using phase 0 to compare the relative frequencies of other phases to determine which exhibit enhanced and which exhibit suppressed MCS activity, it can be seen that phases 2 and 3 are consistently associated with elevated MCS numbers across the domain. For MC12 and MC2, MCS numbers start to increase during phases 6-8 again, while still being slightly suppressed. MCS activity in observations, however, continues to decrease from its peak in phase 2, remaining suppressed in phases 6-8.

This can be compared with the clusters of oceanic convection (not limited to MCSs) in Figure 18 (d,e). The first point of note is that most types of convection filtered here greatly outnumber MCSs. MCSs themselves would be a subset of the anvil types (green and blue), and are not isolated here. Additionally, all types of oceanic convection display a later peak, around phase 5, rather than phase 2 for MCSs. One possible reason for this is that this is only valid for oceanic convection, rather than convection as a whole. A way of investigating this would be to repeat this experiment with oceanic MCSs only, filtered using the land-ocean filter discussed previously.

A similar study into how the MJO influences MCSs over South-East Asia was presented by Crook et al. (2024). This tracking algorithm filtered MCSs under far stricter conditions than in this study, requiring cloud top temperatures below 233K (as opposed to 250K), an area exceeding 10,000km² (as opposed to 2,000km²), and additionally a lifetime requirement where MCSs must persist for at least 6 hours, with mean associated rainfall exceeding 1mm hr⁻¹. Despite this, the results of this study are generally in agreement, with MCS numbers (per day) peaking in earlier phases in most locations.

Crook et al. (2024) also found that the western regions in South-East Asia were more substantially influenced by MJO activity than eastern regions. The investigation into changes to MCS spatial distribution during the MJO below will reveal whether this is the reason for the early peak in MCS activity.

Figures 19, 20 and 21 show how MCS numbers vary relative to the mean through different phases of the MJO, for both simulated atmospheres and observations. Areas of red show areas of enhanced convection, and areas of blue show areas of suppressed convection, where darker colour indicate a larger deviation from the mean. In general, these anomalies are largest over the oceans near islands. The reason for this may be that the time used to generate these plots, 12:00 local time, is one where MCS activity over land is expected to be minimal.

Both simulations and observations show a similar pattern. A region of enhanced MCS activity moves into the domain from the west, before moving into the Pacific Ocean during phases 6 and 7. MCS density anomalies shown in 19, 20 and 21 may be influenced by the numbers of MCSs in the domain, which are shown in 18, or by their areas, shown in 22, since MCS density is a function of the number of times a grid point will be within the bounds of an MCS. If MCSs in a phase are larger on average, each individual system will contain a greater number of grid points, potentially leading to greater anomalies than MCS numbers alone would indicate.

During phase 1, where the area of enhanced convection is expected to be west of the Maritime Continent, there are areas in the centre of the domain with a lower MCS density, which corresponds to the region of dry conditions ahead of the region of enhanced convection shown in World Climate Service (2021). Phase 2 corresponds to the most elevated MCS numbers, as was also found by Crook et al. (2024). Here the area of enhanced convection can be seen entering the west of the domain, however since MCSs are generally small in area, the anomalies themselves are not large in most areas. MC12 is largely in agreement with observations in the placement of enhanced convection, whereas MC2 shows enhanced convection over almost all of the domain. This could be due to the MJO as modelled by the simulations propagating slightly too fast, as was noted by Howard et al. (2024).

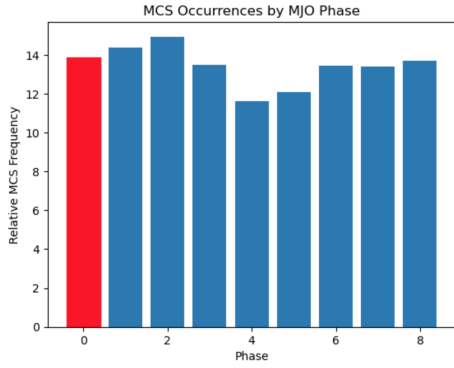
Phases 4 and 5 were shown by the models to have suppressed MCS activity, however many areas of the domain show large positive density anomalies (MC12 and observations). This may be explainable by 22, showing these phases coincide with the largest MCS areas, which would also influence MCS density.

22 shows the way in which MCS characteristics are influenced by the MJO. Despite MCSs peaking in number during the earlier phases, observations show that they do not peak in area until phase 5, with maximum precipitation peaking slightly earlier, when

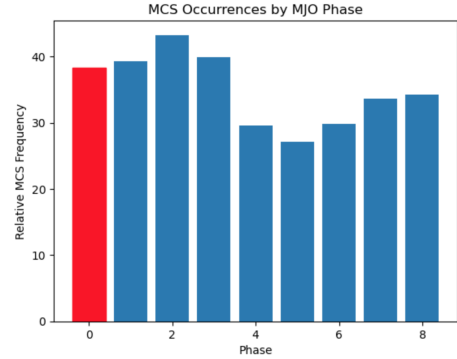
the area of enhanced convection moved over the centre of the domain and areas of land and shallow ocean. This could support the findings of [Huang et al. \(2018\)](#) that land-based MCSs are generally more intense, although it should be noted that intensity is determined by [Huang et al. \(2018\)](#) using a cloud top temperature threshold, rather than any precipitation measurement. This could additionally explain the discrepancy between the behaviour of MCSs compared to oceanic convection as a whole (Figure 18). The oceanic cluster analysis does not consider convection as part of coherent systems in the way the MCS analysis does. So while, in phase 5, the east part of the domain is dominated by fewer, larger MCSs, the oceanic cluster analysis would instead be recognising more frequent instances of anvil-type convection. The median area shows slight variation, however the MJO's influence on MCS area is clearest when considering the range of areas in each phase. The only observed MCSs with areas in excess of 200,000km², without being outliers, were seen in phase 5, with the upper quartile being just over twice that in phase 3. By contrast, MC2 does not show substantial variation in MCS area or maximum precipitation, although does suggest that MCSs are marginally larger during phases 4-6.

MC12 shows the greatest variation in MCS area range. The upper quartile for the phase with the smallest MCSs, phase 3, doubles from around 150,000km² to 300,000km² as the state of the MJO moves into phase 4, while precipitation follows a similar pattern to that of the observations.

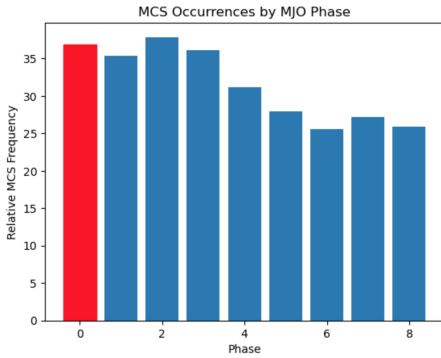
[Virts and Houze \(2015\)](#) investigated the influence of the MJO on MCSs in various regions. In agreement with this study, it was shown that area-averaged precipitation in the Maritime Continent peaks at the same time as maximum precipitation, during phase 4. Additionally, it was shown that MCS areas also show the later peak in phase 5. It should be noted that the areas found by [Virts and Houze \(2015\)](#) were much smaller than many of the MCSs found in this study. This is likely partly due to differing MCS definitions used when filtering them. In addition to a minimum cloud top temperature being less than 220K, an area of precipitation must extend for at least 2000km² and at least 70% of the total area, with an additional core of heavy precipitation accounting for at least 10% of the total cloud area to count as an MCS. The line indicating the median area is of similar magnitude, lying between 10,000km² and 40,000km², slightly smaller than the peak found by [Virts and Houze \(2015\)](#) at just over 45,000km².



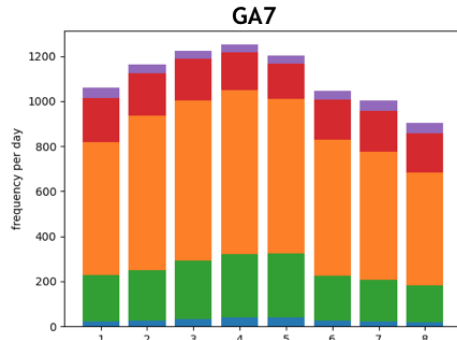
(a) MC12



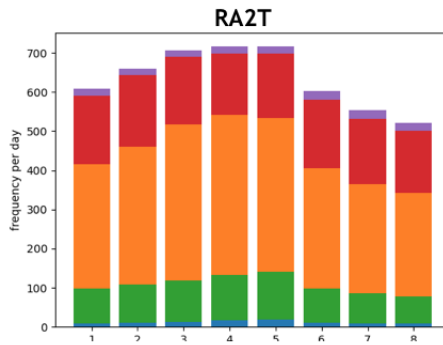
(b) MC2



(c) Observations

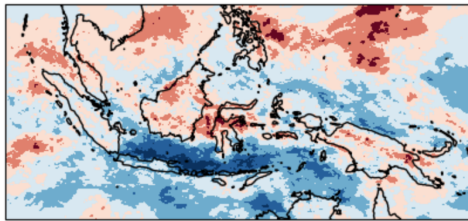


(d) Oceanic Convection (MC12)

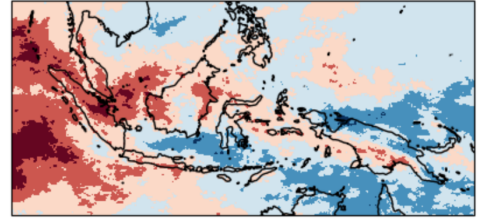


(e) Oceanic Convection (MC2)

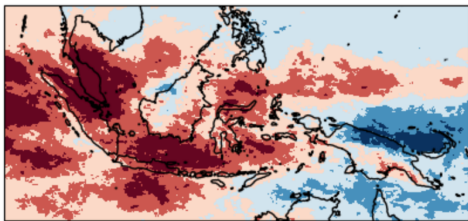
Figure 18: Relative MCS frequency by phase. Note the difference in scales on the y-axis. The different colours for oceanic convection correspond to shallow (purple), congestus (red), deep (yellow), anvil (green) and anvil with extreme re-evaporation (blue)



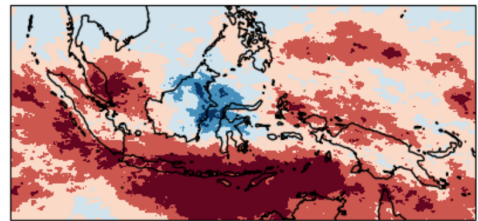
(a) Phase 1



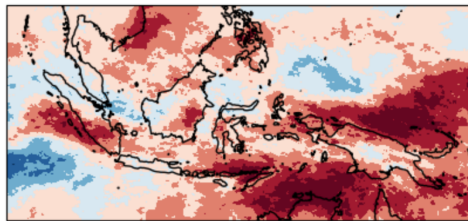
(b) Phase 2



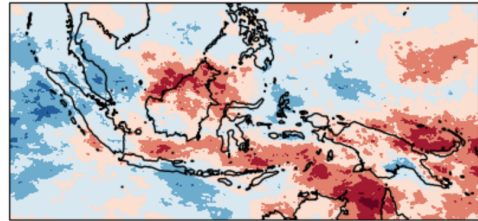
(c) Phase 3



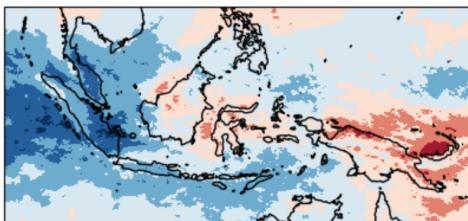
(d) Phase 4



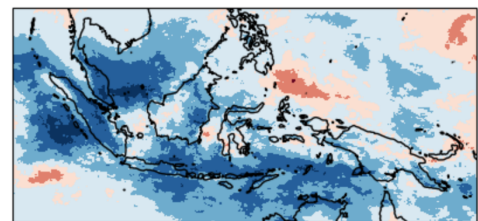
(e) Phase 5



(f) Phase 6

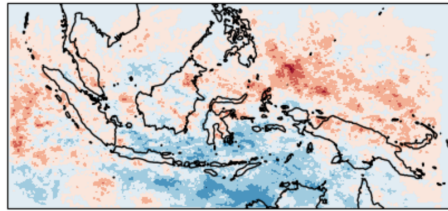


(g) Phase 7

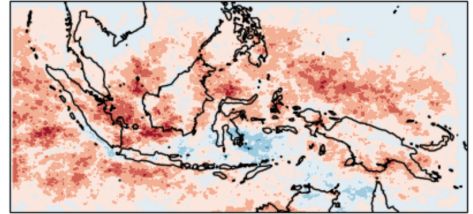


(h) Phase 8

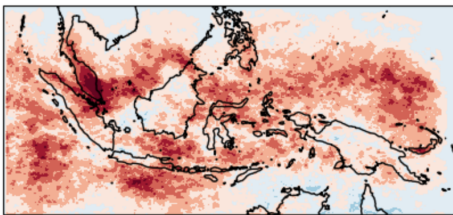
Figure 19: MC12 MCS distribution anomaly by MJO phase at 12:00 local time. Note that areas of red correspond to regions of enhanced convection, and the colour scale across each subfigure is the same



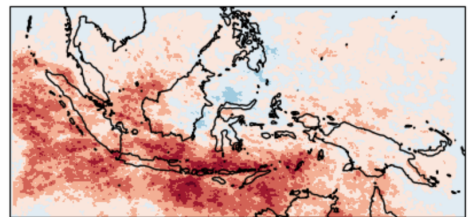
(a) Phase 1



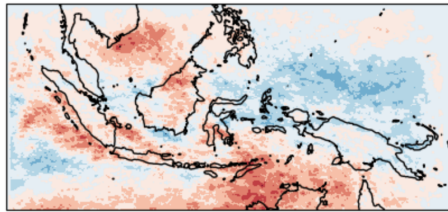
(b) Phase 2



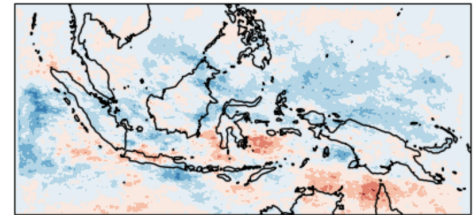
(c) Phase 3



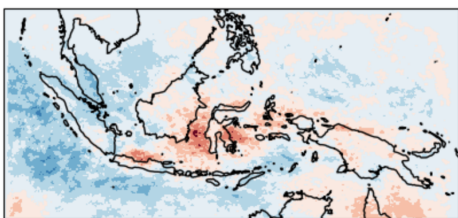
(d) Phase 4



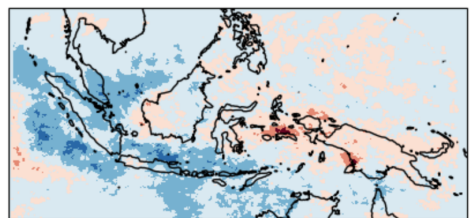
(e) Phase 5



(f) Phase 6

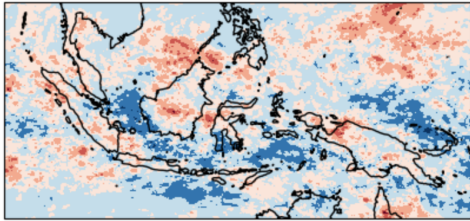


(g) Phase 7

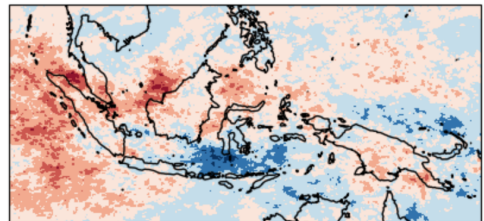


(h) Phase 8

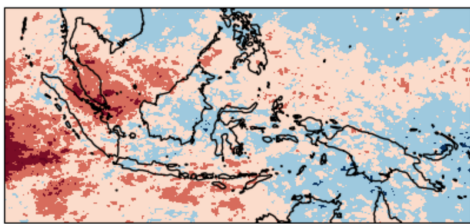
Figure 20: MC2 MCS distribution anomaly by MJO phase at 12:00 local time. Note that areas of red correspond to regions of enhanced convection, and the colour scale across each subfigure is the same



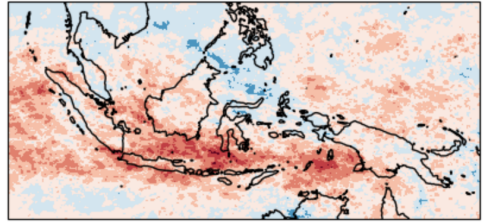
(a) Phase 1



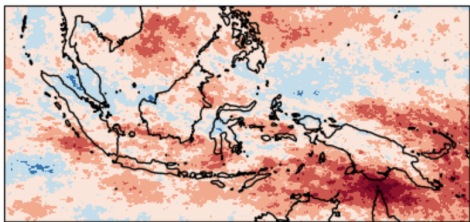
(b) Phase 2



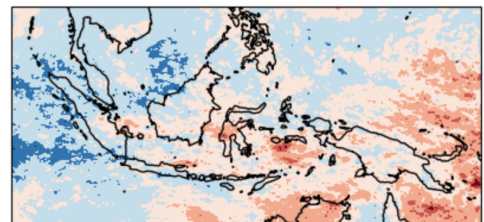
(c) Phase 3



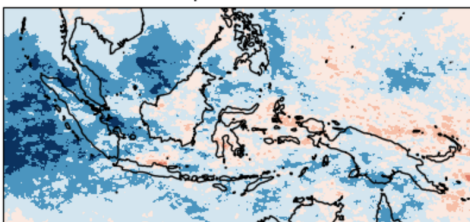
(d) Phase 4



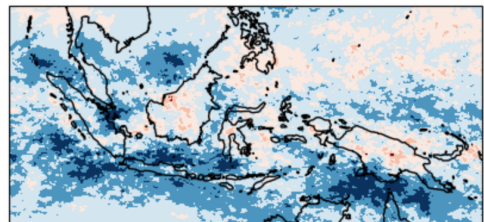
(e) Phase 5



(f) Phase 6

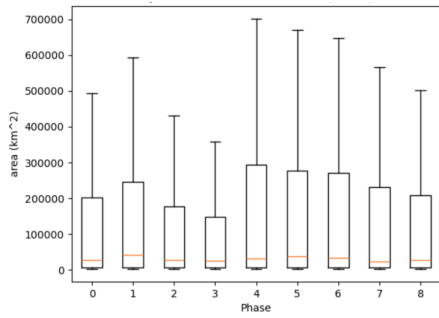


(g) Phase 7

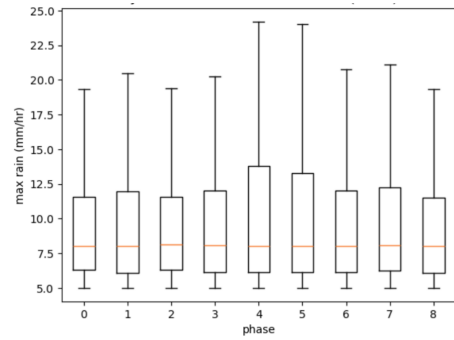


(h) Phase 8

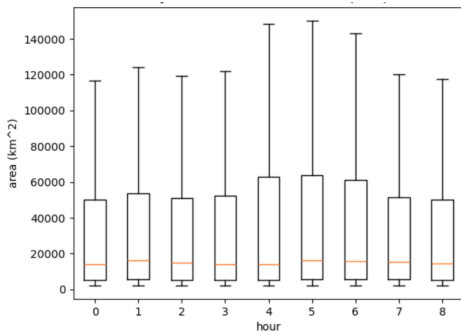
Figure 21: Observations MCS distribution anomaly by MJO phase at 12:00 local time. Note that areas of red correspond to regions of enhanced convection, and the colour scale across each subfigure is the same



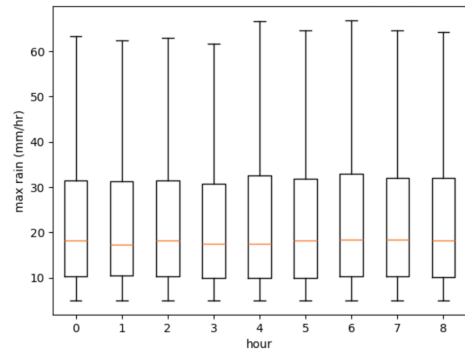
(a) Area (observations)



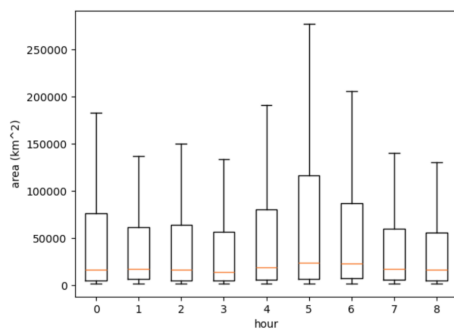
(b) Precipitation (observations)



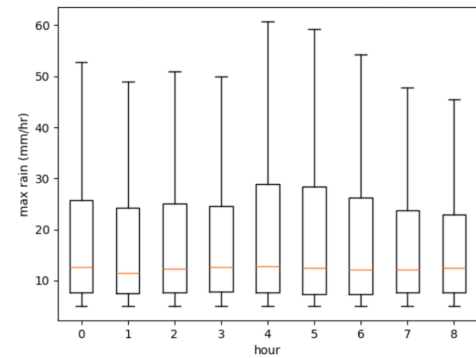
(c) Area (MC2)



(d) Precipitation (MC2)



(e) Area (observations)



(f) Precipitation (observations)

Figure 22: Box plot showing areas and maximum precipitation data separated by MJO phase

7. El Niño Southern Oscillation (ENSO)

7.a *ENSO Methods*

Due to teleconnections, events in one area of the tropics can have long reaching effects. ENSO, despite being characterised by a change in sea surface temperature (SST) in the East Pacific, is the main mode of variability in the tropics varying on an inter-annual basis, with particularly notable effects on the Walker Circulation, and so whether it has any significant effect on the distribution and intensity of MCSs in the Maritime Continent, and particularly how MC2 and MC12 model this, is examined.

During an El Niño year, warm SSTs in the East Pacific result in anomalous rising of air in the eastern branch of the Walker Circulation over this region. This in turn results in the anomalous descent of air over the Maritime Continent, which could be expected to have the effect of suppressing convection, including that associated with MCSs. The opposite is true during a La Niña year, where an increase in MCS activity might be observed.

For both simulations and observations, El Niño, neutral, and La Niña years are separated. The spatial distribution anomalies of MCSs during each of these three conditions calculated by taking the midday mean MCS density for a given ENSO condition and subtracting the midday mean MCS density across all seasons. This anomaly according to both simulations are compared. Note that while the use of MC2 as a benchmark rather than observations (as is done for neutral conditions) may introduce any biases the MC2 data has to conclusions, the observations are only available from 2015 onwards, and so cannot encompass the range of ENSO conditions the simulations can. As a way to verify findings, and to highlight potential biases, both atmospheres are compared to available observations anomaly plots, consisting of two El Niño years (2015 and 2018), and two La Niña years (2016 and 2017). These anomaly plots would show regions of enhanced and suppressed MCS activity, and the average magnitude of the effect ENSO has on MCSs in the Maritime Continent.

As with the study of the diurnal cycle, whether ENSO also affects the intensity of MCSs is examined using box plots for area and maximum precipitation. This time, considering midday conditions, the area and maximum precipitation are recorded for each day in each season for a given ENSO condition.

Given the time scales over which an ENSO event develops, the full event cannot be captured with only the data over Boreal winter, however some development may be seen between December and February, and so anomaly plots for December, January and February are shown separately for each of the atmospheres and observations where this data set is available.

7.b ENSO Results and Analysis

The mean MC2 anomalies during El Niño, neutral, and La Niña years are shown in Figure 23 (middle). Immediately it can be noticed that El Niño and La Niña conditions appear to be near inverses of each other. The decrease (increase) in MCS anomalies in El Niño (La Niña) years is most substantial over oceans, where MCS activity is not as heavily influenced by orographic effects or a strong diurnal cycle. There are some regions of substantially increased MCS activity during El Niño years, with the corresponding area in La Niña years exhibiting a strong decrease in MCS numbers. These are particularly noticeable over Papua New Guinea, Borneo and the Java Sea, and northern Australia. Comparisons to observations (23 bottom) show that for some of these areas, primarily Papua New Guinea, this increase (decrease) in MCS activity during El Niño (La Niña) years could be due to orographic effects over mountains. However, observations do not show the effects over the Java Sea that MC2 does, indicating that this unexpected result in this region could be due to MC2's sensitivity to flow in the domain.

MC12 shows similar results, with fewer MCSs occurring during El Niño years over much of the domain, and with El Niño and La Niña being near inverses of each other. However, MC12 does not show the orographic influence over Papua New Guinea that MC2 does, instead placing a large region of increased MCS activity over the ocean in the east of the domain.

One thing of note is that the ENSO anomalies for MC12 are larger (between -15 and 15) than those of MC2 (between -10 and 10). Comparisons to observations show that the MC2 results are generally closer to the available observations, indicating that MC12 may do a poor job modelling the size of MCS anomalies during El Niño and La Niña years particularly.

Jia et al. (2016) found that the largest precipitation anomalies occur in the east of the domain, and particularly over the ocean directly to the east of the Philippines. This is mostly consistent with the observed MCSs. Anomalies were seen to be low to the south-west of Java and Sumatra, with some of the largest anomalies being seen near the Philippines. The region in Papua New Guinea where ENSO appears to have the opposite effect than it has on the rest of the domain was only found to appear with at least 90% confidence during moderate El Niño years, and not at all during strong El Niño years or La Niña years. In further work, the strong El Niño year in the observations data set could be separated from the weak El Niño year to see if the findings of Jia et al. (2016) reflected in the MCS distributions.

24 shows MCS area and maximum precipitation separated by ENSO condition. It shows that, for the MC2 data, ENSO does not have a significant effect on the intensity

of MCSs, but only on their frequency and spatial distribution. Similar results were noted for MC12 and the observations, but have not been included here.

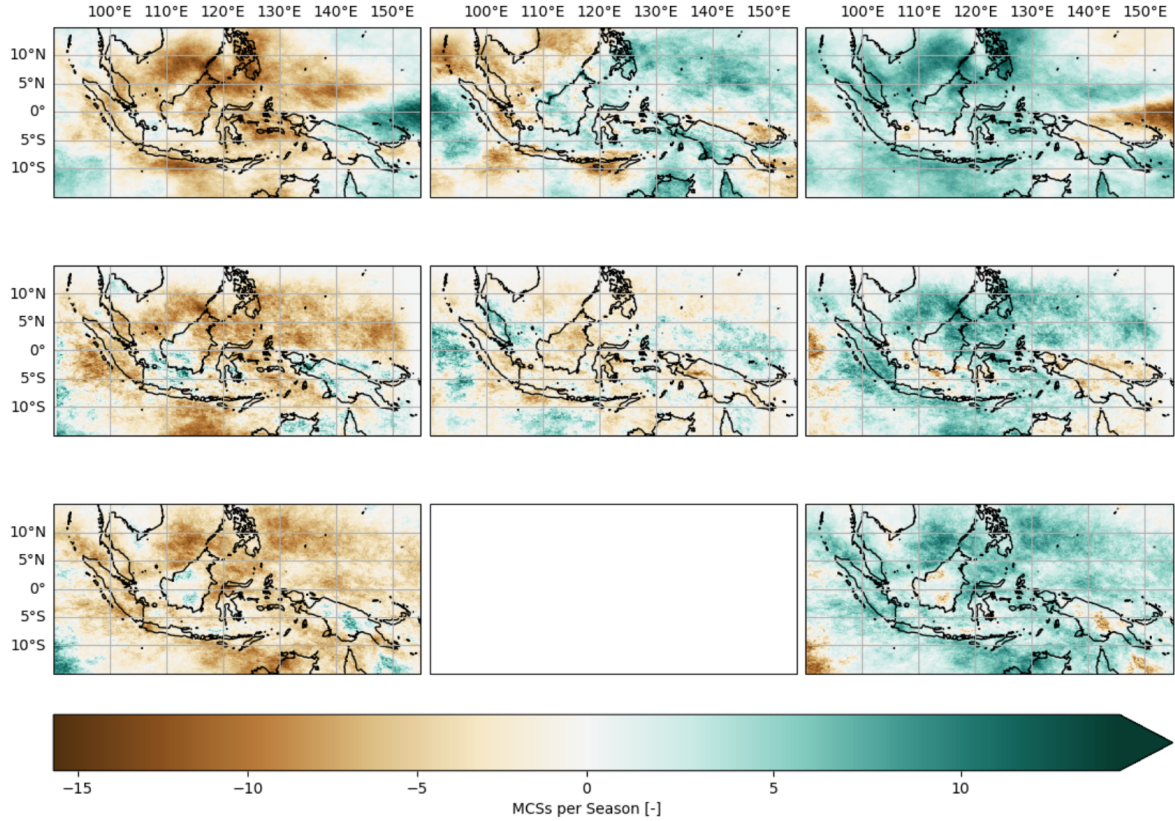


Figure 23: MCS distribution anomaly by ENSO phase, for El Niño (left), neutral (centre), and La Niña (right), and for MC12 (top), MC2 (middle), and observations (bottom). Note that there is no plot for observations in neutral conditions as there is no such data available.

For 12:00 local time, it appears that El Niño results in a large decrease in MCS frequency in most places in the domain. Over the Maritime Continent, the domain-averaged anomaly in MCS activity during El Niño years is around -3 MCSs per season. With a domain-averaged mean MCS frequency of 17 per season, this would imply that the magnitude of the average anomaly is 18% of the mean number of MCSs in a given location, indicating a significant decrease.

In order to perform a statistical test to determine whether this decrease is statistically significant, MCS frequency data for a given point is assumed to be normally distributed. As there are only ten years in the data set, normally distributed data cannot be confirmed with absolute certainty, but it is possible to check whether it is likely to be normally distributed. Five points are chosen such that a range of different locations and conditions in the domain are represented. For each year, the number of MCSs in each location is recorded and plotted in a histogram. While somewhat difficult to interpret due to the

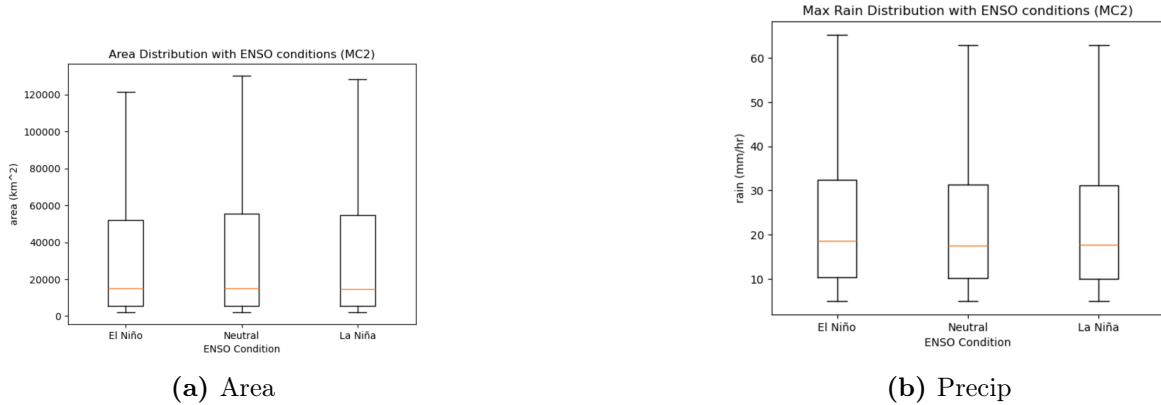


Figure 24: MC2 area and maximum precipitation distributions separated by ENSO state

limited number of time points, MCS frequency in the selected points did appear to be taking the shape of a normal distribution (see Appendix A), providing evidence that a hypothesis test is applicable here.

For each point in the domain, at 12:00 local time, there is a mean MCS frequency, calculated during the section on MCS diurnal cycle, and a sample representing MCS numbers in each El Niño year, of size four. From here it is simple to calculate the mean and standard deviation for the El Niño sample. For each point in the domain, a hypothesis test is set up as follows:

Let μ_p be the mean of the population, and let μ_s be the mean of the sample. The sample size $N=4$ gives $N-1=3$ degrees of freedom, and since $N < 30$, and that the standard deviation of the population mean is unknown, a single sample t-test is the most suitable [Hogg and Craig \(1995\)](#). A crucial assumption made in conducting a single sample t-test is that the mean over the 10 years in MC2’s data set is a reasonable approximation of the mean that would be calculated if MC2 were run over all years. The 10 years were deliberately chosen to encompass as large a range and number of combinations of ENSO conditions and MJO phases as possible, so this is considered a justifiable assumption to make. Note that after this point, this 10-year mean is referred to as the population mean, under the assumption that any differences between the two are negligible. Given that the intent is to test whether El Niño results in a decrease in MCS activity, rather than testing for any change, a one-tailed test is used, specifically examining the left tail. The null hypothesis H_0 and the alternative hypothesis H_1 , which we hope to be able to reject the null hypothesis in favour of, can then be defined such that

$$H_0 : \mu_s = \mu_p$$

$$H_1 : \mu_s < \mu_p$$

for any given point in the domain. A confidence level of 90% is chosen so that the probability of an incorrect rejection of the null hypothesis is 0.1 for a given grid point, which is sufficiently low to show whether El Niño has a statistically significant influence on MCS density over the domain as a whole. Taking this confidence level gives a t-value (from table) of -1.64, where the negative value is taken as it is a left tail test. For each point in the domain, the standard deviation (σ) is calculated using

$$\sigma = \sqrt{\frac{\sum_1^N (x_i - \mu)^2}{N}}$$

Hogg and Craig (1995). From here the critical value T_c can then be calculated as

$$T_c = \frac{\mu_s - \mu_p}{\frac{sd}{N-1}}$$

Hogg and Craig (1995). Each T_c in the domain is then compared to the t-value. Wherever $T_c < t$ -value, the null hypothesis can be rejected. Applying this test to each point in the whole domain, and applying a mask to the result to distinguish areas where H_0 can be rejected from areas where it cannot be results in Figure 25 (a) Many areas where there

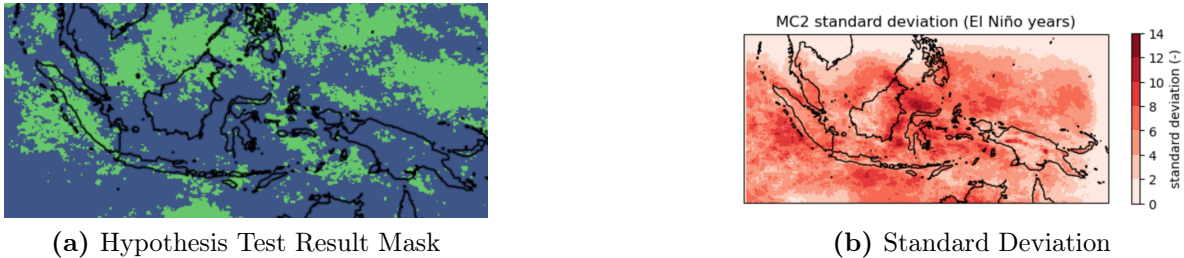


Figure 25: Results of the hypothesis test outlined in the main text. Areas in green in the mask correspond to areas where H_0 can be rejected

is enough evidence to say that El Niño events result in a statistically significant negative anomaly in MCS numbers coincide with those where the negative anomaly is deepest. To investigate this, each point in the H_0 rejection mask was taken in turn. Points where H_0 can be rejected are separated from those it can't, to allow an investigation into whether there are substantial differences between the two groups. Both groups were then plotted as in 26. This shows two distinctly different groups, with group 1, where there was insufficient evidence to reject H_0 , showing the members of this group on average being much closer to the population mean (anomaly closer to 0) than in the H_0 rejection group (group 2), with an average anomaly of -5 MCSs per season.

Comparing with the standard deviation plot suggests that in areas where a deep anomaly does not correspond to an area where H_0 can be rejected, a high standard deviation often leads to the conclusion that the sample mean cannot be considered lower than the population mean with a high enough certainty; in other words since the number of MCSs in the El Niño years varies so greatly in these locations, it is possible that had more years been sampled, the mean number of MCSs in El Niño years may have not been significantly different to the population mean.

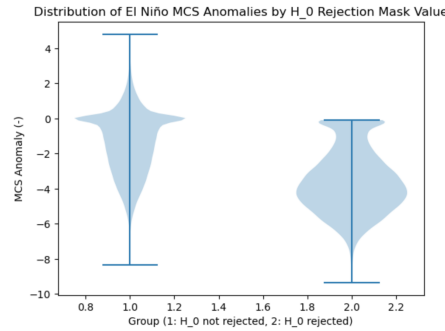


Figure 26: Violin plot showing distributions in anomaly magnitude when H_0 cannot, and when H_0 can, be rejected

The way an El Niño event develops was also investigated. 27 shows, for MC2 and observations, anomalies are initially small and begin in December, before deepening through January and February, where negative MCS anomalies cover most of the domain, with these deviations from the mean generally being large.

As was noted previously, El Niño most substantially affects oceanic regions, and this is reflected in 27 with anomalies being low, or even positive, over land-based areas. In particular, there is a region in observations of increased MCS activity in Papua New Guinea, which deepens over the season. Given its proximity to the mountain ridge, it's plausible that this is due to orographic effects.

Jia et al. (2016) noted that significant 850hPa wind anomalies are only present in the Maritime Continent during strong El Niño events. During these years, wind coming from surrounding oceans could bring moisture that, in addition to lifting as a result of orography, could contribute to this increase in MCS activity, although for much of Papua New Guinea they noted these anomalies were not statistically significant. In future work, investigations into how El Niño affects the drivers of convection, split into land and ocean subsets, could provide insight into why this effect is observed.

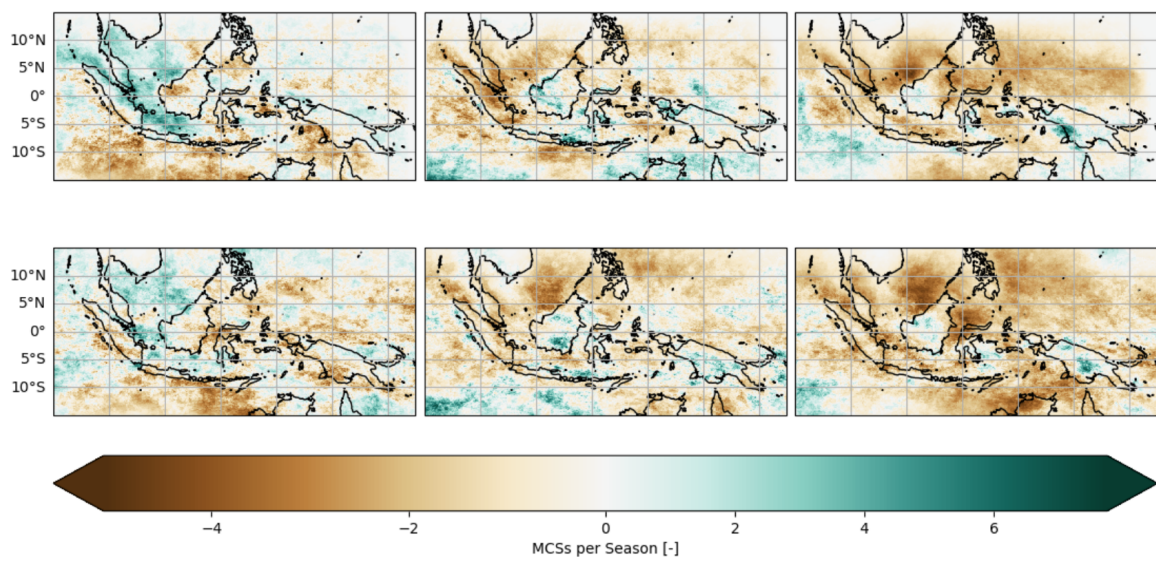


Figure 27: MCS anomaly in each month of an El Niño season for MC2 (top) and MC12 (bottom), relative to the mean. Note that colour scale is in MCSs per month, rather than MCSs per season.

8. Further Work

This study has mainly considered the statistics of MCS occurrences, however plotting the vertical heating and moistening profiles would allow for direct comparisons with the clusters introduced in Section 2. It is likely that the vertical profiles of MCSs would most closely resemble the anvil type clusters, rather than that of deep, congestus or shallow, as the MCSs identified in this study are a subset of these types.

Doing this could additionally provide insight into some of the more surprising results, such as whether modulations in heating and moistening may be partly responsible for the equal and opposite effects of El Niño and La Niña on MCS distribution, while area and maximum precipitation remain relatively unchanged.

The techniques used in this study could also be used to construct a statistical MCS forecast. Given regions where the influence of each mode of variability is statistically significant, and their average anomalies from the 10-year mean in those locations, the mean could be modulated by applying each anomaly mask in turn. This would give a prediction for mean MCS distribution for a given time, MJO phase and ENSO state. From there, comparisons with data from periods not in the 10 year set could be made to assess the ability of the statistical forecast to predict MCS distribution.

To measure this, several metrics could be used. For example, an accuracy metric would give the fraction of grid squares where the forecast was correct. This could be misleadingly high over the regions of open ocean where MCSs were shown to be relatively rare. To avoid drawing a conclusion that the forecast is better at predicting MCSs than it is in reality, other metrics can be considered alongside accuracy, such as the fraction of observed MCSs that were predicted by the model, and conversely the fraction of forecast MCSs that were not observed.

Ideally, this would be done with observations, and for the statistical forecast to be shown to be a useful tool, it would need to be comparatively or more skilled than a medium-range forecast. However, due to the number of observations available to this study being low, MC2 has been used to demonstrate how the statistical forecast may work (see appendix B).

9. Conclusions

Throughout this study, we have investigated the ability of the two simulated atmospheres to form MCSs by comparing the spatial distributions, areas and maximum associated precipitation of those MCSs identified by the filtering algorithm with those identified in the available observations. The filtering algorithm was additionally verified by comparisons to previous studies into MCSs in the region, such as [Chen and Houze Jr \(1997\)](#) and

[Mohr and Zipser \(1996\)](#). We then moved on to investigating three modes of variability in the tropics: the diurnal cycle, the MJO and ENSO.

It was found that MC2 generally performs similarly to observations, with mean MCS numbers in the domain often being close to the observed number, with interactions with orography and warm SSTs reflected. However, there was some evidence to suggest that MC2 may be too sensitive to interactions between flow and orography, shown in the early morning peak in land-based MCS activity that was not seen in MC12 or observations. The fraction of precipitation in the Maritime Continent using observations was consistent with the study of [Feng et al. \(2021\)](#), with most days seeing >50% of their total precipitation originating from MCSs. MC12, by contrast, produced up to 80% fewer MCSs than MC12 and observations, however the MCSs that MC12 did produce were an order of magnitude too large and concentrated in the middle of the domain with less sensitivity to orography, suggesting that MC2 is better able to produce realistic MCSs within the domain.

Two peaks in average MCS numbers were seen for the two simulated atmospheres and observations, corresponding to the ocean peak in the early morning and the land peak in mid-late afternoon found by [Huang et al. \(2018\)](#). Despite MC12 producing substantially fewer MCSs, both simulated atmospheres and the observations show similar variability over the average day, with the troughs in MCS activity showing 74 – 77% the activity during peak times. While MC2 did not capture the magnitude of the ocean peak, it did a good job placing the peaks at the same time as the observed peaks. On the other hand, MC12 did produce two similarly sized peaks, however its land peak was late, being closer to 20:00 local time.

Neither simulated atmosphere captured the way MCS area and maximum precipitation vary through the day; the largest MCSs produced by MC2 and observations were detected at 18:00 and 12:00 respectively, both of which are seemingly at odds with [Mohr and Zipser \(1996\)](#), who found that MCSs occurring in the early morning are frequently larger, oceanic systems. One possible reason for the discrepancy was suggested to be that the findings of [Mohr and Zipser \(1996\)](#) regarding differences between land-based and oceanic MCSs mostly apply to continental and open ocean MCSs. MC12 showed the greatest diurnal variability in both area and precipitation, neither of which are realistic when compared to observations, but there were some similarities between these results and those of previous studies ([Mohr and Zipser \(1996\)](#), [Huang et al. \(2018\)](#)) that showed MCSs are often larger in the morning, but are more intense in the evening.

All data sets were then split by MJO phase, and it was found that MCS activity peaks in phases 2 and 3, with other phases in observations and MC12 being suppressed, and a slight enhancement in phases 6-8 for MC2. By contrast, oceanic convection as a whole does not peak until phase 5. This was likely due to the way this study only

considers organised convection, and MCSs were also found to be largest in area in phase 5, for both simulated atmospheres and the observations. In all data sets, the signal of the MJO passing through the Maritime Continent could be distinctly seen. In addition to influencing MCS spatial distribution, it was also found that the MJO affects MCS area and, to a lesser extent, maximum associated precipitation. As previously noted, areas peak in phase 5, with maximum precipitation peaking slightly earlier in phase 4. MC2 showed less variability in intensity as defined in this study than both MC12 and observations.

Finally, modulations to MCS activity as a result of ENSO were investigated. It was found that, for both simulated atmospheres and available observations, El Niño and La Niña mirror each other, with magnitudes of MCS number anomalies in most parts of the domain being equal and opposite. It was also shown that the anomalies deepen gradually during an ENSO growth phase. Unlike the MJO, ENSO was not shown to have a substantial influence on MCS size and maximum precipitation. A hypothesis test carried out on the MC2 El Niño data showed that, at 90% confidence, there are several regions through the Maritime Continent where El Niño has a statistically significant influence on MCS numbers.

References

- Chen, S. S., and R. A. Houze Jr, 1997: Diurnal variation and life-cycle of deep convective systems over the tropical pacific warm pool. *Quarterly Journal of the Royal Meteorological Society*, **123** (538), 357–388, doi:<https://doi.org/10.1002/qj.49712353806>, URL <https://rmets.onlinelibrary.wiley.com/doi/abs/10.1002/qj.49712353806>, <https://rmets.onlinelibrary.wiley.com/doi/pdf/10.1002/qj.49712353806>.
- Crook, J., and Coauthors, 2024: Impact of the Madden–Julian oscillation and equatorial waves on tracked mesoscale convective systems over southeast Asia. *Quarterly Journal of the Royal Meteorological Society*, **150** (760), 1724–1751, doi:<https://doi.org/10.1002/qj.4667>, URL <https://rmets.onlinelibrary.wiley.com/doi/abs/10.1002/qj.4667>, <https://rmets.onlinelibrary.wiley.com/doi/pdf/10.1002/qj.4667>.
- Dai, A., and T. M. L. Wigley, 2000: Global patterns of enso-induced precipitation. *Geophysical Research Letters*, **27** (9), 1283–1286, doi:<https://doi.org/10.1029/1999GL011140>, URL <https://agupubs.onlinelibrary.wiley.com/doi/abs/10.1029/1999GL011140>, <https://agupubs.onlinelibrary.wiley.com/doi/pdf/10.1029/1999GL011140>.
- Feng, Z., and Coauthors, 2021: A global high-resolution mesoscale convective system database using satellite-derived cloud tops, surface precipitation, and tracking. *Journal of Geophysical Research: Atmospheres*, **126** (8), e2020JD034202, doi:<https://doi.org/10.1029/2020JD034202>, URL <https://agupubs.onlinelibrary.wiley.com/doi/abs/10.1029/2020JD034202>, e2020JD034202 2020JD034202, <https://agupubs.onlinelibrary.wiley.com/doi/pdf/10.1029/2020JD034202>.
- Gottschalck, J., and Coauthors, 2010: A framework for assessing operational madden–julian oscillation forecasts: A clivar mjo working group project. *Bulletin of the American Meteorological Society*, **91** (9), 1247 – 1258, doi:10.1175/2010BAMS2816.1, URL https://journals.ametsoc.org/view/journals/bams/91/9/2010bams2816_1.xml.
- Hendon, H. H., and B. Liebmann, 1994: Organization of convection within the madden–julian oscillation. *Journal of Geophysical Research: Atmospheres*, **99** (D4), 8073–8083, doi:<https://doi.org/10.1029/94JD00045>, URL <https://agupubs.onlinelibrary.wiley.com/doi/abs/10.1029/94JD00045>, <https://agupubs.onlinelibrary.wiley.com/doi/pdf/10.1029/94JD00045>.
- Hogg, R. V., and A. T. Craig, 1995: *Introduction to Mathematical Statistics*. Prentice-Hall.

- Holton, J. R., and G. J. Hakim, 2013: Chapter 11 - tropical dynamics. *An Introduction to Dynamic Meteorology (Fifth Edition)*, J. R. Holton, and G. J. Hakim, Eds., fifth edition ed., Academic Press, Boston, 377–411, doi:<https://doi.org/10.1016/B978-0-12-384866-6.00011-8>, URL <https://www.sciencedirect.com/science/article/pii/B9780123848666000118>.
- Houze Jr., R. A., 2004: Mesoscale convective systems. *Reviews of Geophysics*, **42** (4), doi:<https://doi.org/10.1029/2004RG000150>.
- Howard, E., S. Woolnough, N. Klingaman, D. Shipley, C. Sanchez, S. C. Peatman, C. E. Birch, and A. J. Matthews, 2024: Evaluation of multi-season convection-permitting atmosphere – mixed-layer ocean simulations of the maritime continent. *Geoscientific Model Development*, **17** (9), 3815–3837, doi:10.5194/gmd-17-3815-2024, URL <https://gmd.copernicus.org/articles/17/3815/2024/>.
- Huang, X., C. Hu, X. Huang, Y. Chu, Y.-h. Tseng, G. J. Zhang, and Y. Lin, 2018: A long-term tropical mesoscale convective systems dataset based on a novel objective automatic tracking algorithm. *CLIMATE DYNAMICS*, **51** (7-8), 3145–3159, doi:10.1007/s00382-018-4071-0.
- Jia, X., J. Ge, and S. Wang, 2016: Diverse impacts of enso on wintertime rainfall over the maritime continent. *International Journal of Climatology*, **36** (9), 3384–3397, doi: <https://doi.org/10.1002/joc.4562>, URL <https://rmets.onlinelibrary.wiley.com/doi/abs/10.1002/joc.4562>, <https://rmets.onlinelibrary.wiley.com/doi/pdf/10.1002/joc.4562>.
- Lu, J., T. Li, and L. Wang, 2021: Precipitation diurnal cycle over the maritime continent modulated by the climatological annual cycle. *Journal of Climate*, **34** (4), 1387 – 1402, doi:10.1175/JCLI-D-20-0130.1, URL <https://journals.ametsoc.org/view/journals/clim/34/4/JCLI-D-20-0130.1.xml>.
- Markowski, P., and Y. Richardson, 2010: *Mesoscale Meteorology in Midlatitudes*. Wiley-Blackwell.
- Mohr, K., and E. Zipser, 1996: Mesoscale convective systems defined by their 85-ghz ice scattering signature: Size and intensity comparison over tropical oceans and continents. *MONTHLY WEATHER REVIEW*, **124** (11), 2417–2437, doi:10.1175/1520-0493(1996)124<2417:MCSDBT>2.0.CO;2.
- Muetzelfeldt, M. R., R. S. Plant, H. M. Christensen, Z. Zhang, T. Woollings, Z. Feng, and P. Lid, 2024: Environmental conditions affecting global mesoscale convective system occurrence. -, manuscript in preparation.

- Nesbitt, S. W., R. Cifelli, and S. A. Rutledge, 2006: Storm morphology and rainfall characteristics of trmm precipitation features. *Monthly Weather Review*, **134** (10), 2702 – 2721, doi:10.1175/MWR3200.1, URL <https://journals.ametsoc.org/view/journals/mwre/134/10/mwr3200.1.xml>.
- NOAA, 2014: The Walker Circulation: ENSO’s atmospheric buddy. ENSO diagram, accessed 27/8/24, <https://www.climate.gov/news-features/blogs/enso/walker-circulation-ensos-atmospheric-buddy#>.
- Peatman, S. C., A. J. Matthews, and D. P. Stevens, 2014: Propagation of the maden–julian oscillation through the maritime continent and scale interaction with the diurnal cycle of precipitation. *Quarterly Journal of the Royal Meteorological Society*, **140** (680), 814–825, doi:https://doi.org/10.1002/qj.2161, URL <https://rmets.onlinelibrary.wiley.com/doi/abs/10.1002/qj.2161>, <https://rmets.onlinelibrary.wiley.com/doi/pdf/10.1002/qj.2161>.
- Peters, J. M., D. R. Chavas, C.-Y. Su, H. Morrison, and B. E. Coffey, 2023: An analytic formula for entraining cape in midlatitude storm environments. *Journal of the Atmospheric Sciences*, **80** (9), 2165 – 2186, doi:10.1175/JAS-D-23-0003.1, URL <https://journals.ametsoc.org/view/journals/atsc/80/9/JAS-D-23-0003.1.xml>.
- Virts, K. S., and R. A. Houze, 2015: Variation of lightning and convective rain fraction in mesoscale convective systems of the mjo. *Journal of the Atmospheric Sciences*, **72** (5), 1932 – 1944, doi:10.1175/JAS-D-14-0201.1, URL <https://journals.ametsoc.org/view/journals/atsc/72/5/jas-d-14-0201.1.xml>.
- Wallace, J. M., and P. V. Hobbs, 2006: *Atmospheric Science*. Elsevier Inc.
- Wheeler, M. C., and H. H. Hendon, 2004: An all-season real-time multivariate mjo index: Development of an index for monitoring and prediction. *Monthly Weather Review*, **132** (8), 1917 – 1932, doi:10.1175/1520-0493(2004)132<1917:AARMMI>2.0.CO;2, URL https://journals.ametsoc.org/view/journals/mwre/132/8/1520-0493_2004_132_1917_aarmmi_2.0.co_2.xml.
- Worku, L. Y., A. Mekonnen, and C. J. Schreck III, 2019: Diurnal cycle of rainfall and convection over the maritime continent using trmm and isccp. *International Journal of Climatology*, **39** (13), 5191–5200, doi:https://doi.org/10.1002/joc.6121, URL <https://rmets.onlinelibrary.wiley.com/doi/abs/10.1002/joc.6121>, <https://rmets.onlinelibrary.wiley.com/doi/pdf/10.1002/joc.6121>.

World Climate Service, 2021: What is the Madden-Julian Oscillation. MJO summary, accessed 12/8/24, <https://www.worldclimateservice.com/2021/09/20/madden-julian-oscillation/>.

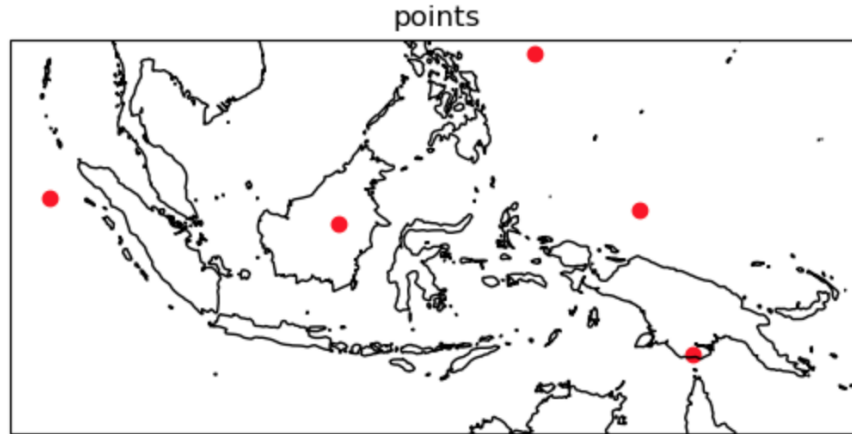


Figure 28: The five points chosen to represent the domain as a whole.

10. Appendix A: Applicability of Hypothesis Test

As discussed when setting up the hypothesis test for the influence of El Niño on MCS distribution, for such a test to be applicable, the distribution of MCS numbers for each grid square must be normally distributed.

Five points were chosen to represent the domain as a whole (28). These included regions over land and over ocean, spread out across the Maritime Continent. Over all ten years in the data set, the number of MCSs recorded in these grid squares over the season, and a histogram is plotted. While the distributions of all points were plotted separately, the proximity to a normal distribution was clearest when the distributions of all five points are combined (29). A slight skew in the data is noted, but this could be due to the selection of points; MCSs are relatively common for all points except that north-east of the Philippines. It should be noted that the assumption being made that this distribution is consistent across all points in the domain, which is a reasonable one given the selection to include a variety of points in the domain.

distribution of MCS # across 10 seasons for 5 random grid points

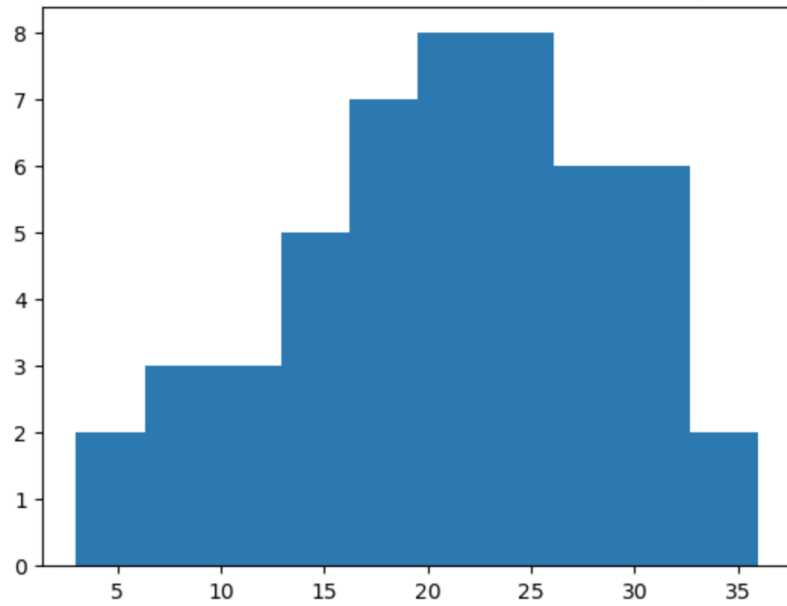


Figure 29: Distribution of MCS numbers for the points specified in [28](#)

11. Appendix B: Statistical MCS Forecasting Model Concept

It has been noticed throughout this project that the spatial distribution of MCSs is variable under the main modes of variability. To test this in a quantifiable way, an statistical tool can be constructed that would operate as an inverse of the MCS detection algorithm introduced in this study, by taking information about the time, MJO phase and ENSO state and producing predicted MCS densities throughout the domain. Using midnight, El Niño and MJO phase 5 as an example, similar hypothesis tests are conducted as in the ENSO section (2-tail, 90% significance) and a mask representing areas of statistical significance, along with the respective anomalies, are constructed. As an initial demonstration of the concept, the masks and anomalies are simply stacked:

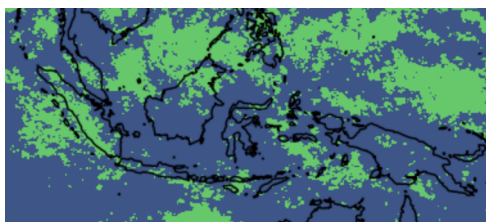
$$mask(total) = mask(hour) + mask(mjo) + mask(enso)$$

$$mcs_{dist} = mean + anomaly(hour(mask)) + anomaly(mjo(mask)) + anomaly(enso(mask))$$

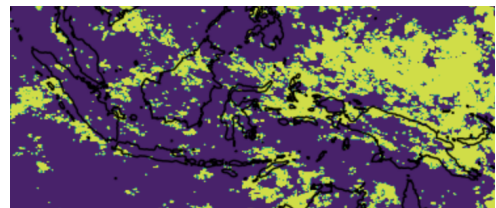
where

$$anomaly = MCSs(condition) - MCS(mean)$$

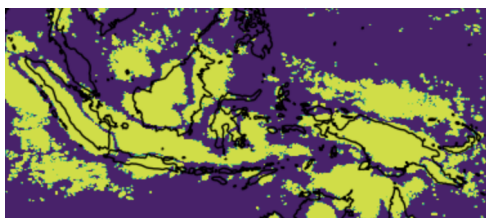
It should be noted here that this method assumes that the modes of variability are independent and do not substantially influence each other's behaviour. This assumption would be difficult to relax, and is considered a reasonable one to make for this initial demonstration, but work would need to be done to either verify the assumption is reasonable, or find a methodology that will relax it if this were to be implemented.



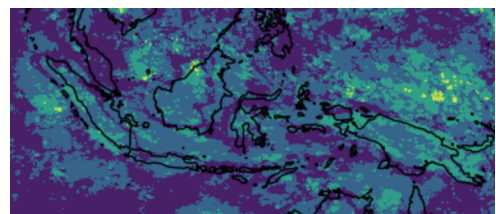
(a) El Niño Mask



(b) MJO mask (phase 5)



(c) Diurnal mask (00:00)



(d) Total mask

Figure 30: Masks of statistical significance for each mode of variability, with total mask also shown (d)

Figure 30 (d) shows all areas of statistical significance for the three modes of variability. Areas of yellow indicate that all three influence MCS density in a statistically significant way. Areas of dark blue show areas where no mode of variability affects MCS density significantly, and so the mean in these areas should not be modified at all.

MCS numbers under each mask are then modified by the respective anomalies from the 10-year mean. Computing this adjusts the mean (31 left) to a seasonal mean MCS density prediction (31). When comparing to the mean MCS density under these conditions (Figure 32) this initial result looks promising, however it should be noted that this may look misleadingly accurate due to the fact that the data in 32 was used to generate the masks and calculate the anomalies within them, so no conclusions can be drawn based on this initial demonstration.

If this statistical tool were to be constructed, it would be most useful if observations data were used (MC2 was used for this demonstration due to there not being enough observations data to construct the hypothesis tests) and compared to a year not used in the tests. Assessing its performance would provide insight into how much of the variability seen in MCS distribution can be explained by the three main modes of variability in the tropics, and if successful could reduce the reliance on physical models that often do a poor job accurately capturing convection, especially with lead times weeks in advance. For the statistical tool to be considered useful in forecasting, it would need to out perform a mid-range forecast.

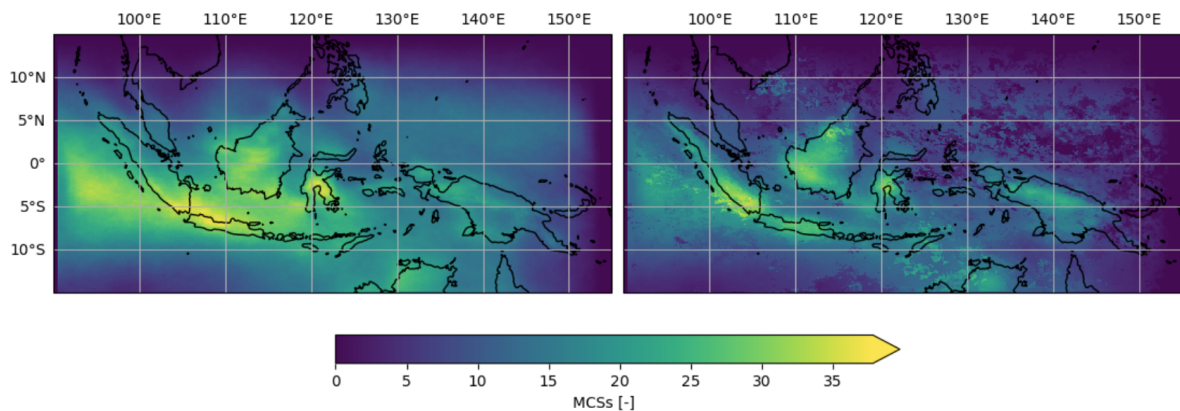


Figure 31: Change to predicted MCS spatial distributions, given the time is 00:00, in an El Niño year, during MJO phase 5

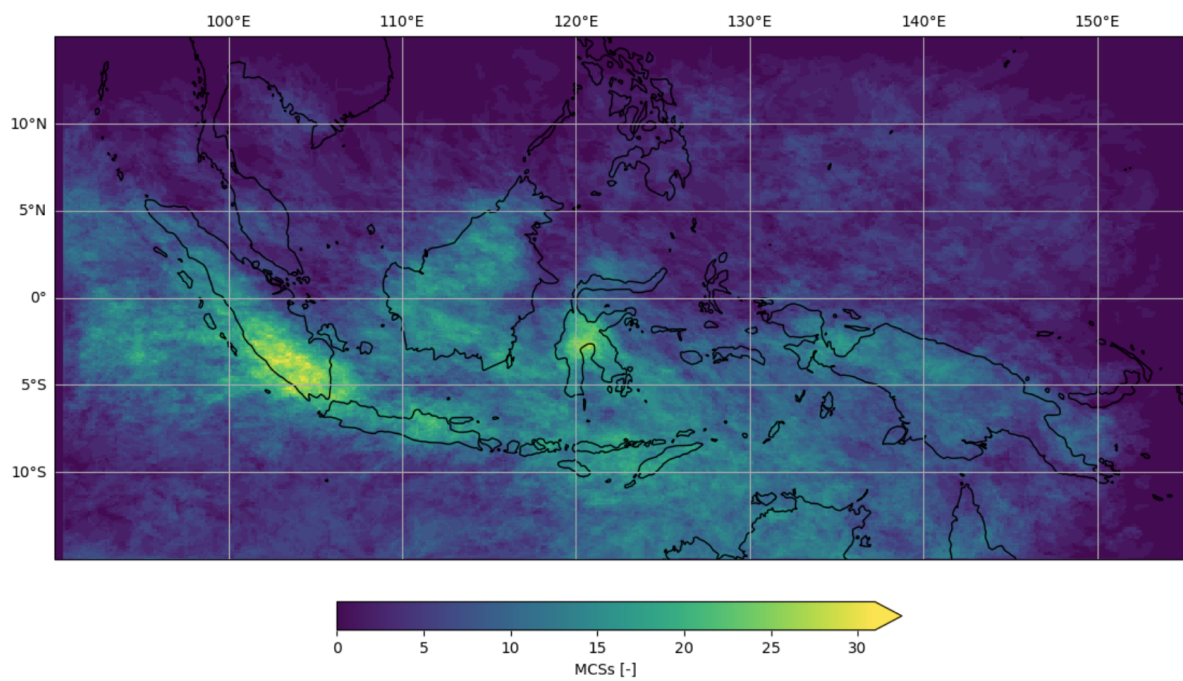


Figure 32: The mean of all days in MJO phase 5 in El Niño years, taken at midnight